Scholars' Mine

Masters Theses

Student Theses and Dissertations

1965

An x-ray study of the lead zirconate-bismuth ferrate system

Pen-chu Chou

Follow this and additional works at: https://scholarsmine.mst.edu/masters_theses

Part of the Chemistry Commons

Department:

Recommended Citation

Chou, Pen-chu, "An x-ray study of the lead zirconate-bismuth ferrate system" (1965). *Masters Theses*. 5717.
https://scholarsmine.mst.edu/masters_theses/5717

This thesis is brought to you by Scholars' Mine, a service of the Missouri S&T Library and Learning Resources. This work is protected by U. S. Copyright Law. Unauthorized use including reproduction for redistribution requires the permission of the copyright holder. For more information, please contact scholarsmine@mst.edu.

244

101p

AN X-RAY STUDY OF THE LEAD ZIRCONATE-BISMUTH FERRATE SYSTEM

by

PEN-CHU CHOU -1936

A

THESIS

submitted to the faculty of the

UNIVERSITY OF MISSOURI AT ROLLA

in partial fulfillment of the work required for the

Degree of

MASTER OF SCIENCE IN CHEMISTRY

Rolla, Missouri

1965

T1832
c.1

Approved by

W. J. James (Advisor) Robert Gerson

G. E. Lorey W. P. Tappmeyer

117720

ABSTRACT

The lead zirconate-bismuth ferrate system was studied employing x-ray and microscopic analysis. Samples were prepared by sintering stoichiometric mixtures of the corresponding oxides followed by air quenching. The results of the analyses show the system to be probably solid solutions over the entire compositional range, although small amounts of other phases are present in some regions.

X-ray data indicate a multiple cell, orthorhombic phase, to exist over the range 100-30 mole percent $PbZrO_3$. From 100-82 mole percent $PbZrO_3$, the addition of $BiFeO_3$ reduces the distortion of the phase such that a nearly cubic x-ray pattern is obtained at approximately 80 mole percent $PbZrO_3$. In the same range dielectric measurements suggest antiferroelectric properties. The nearly cubic phase is also confirmed by a minimum in a plot of Curie points versus composition.

From 80-30 mole percent $PbZrO_3$ the structure is only slightly distorted from that at 80 mole percent $PbZrO_3$. In the range 80-50 mole percent $PbZrO_3$, the system is apparently ferroelectric. Samples of composition greater than 50 mole percent $BiFeO_3$ are too conductive for meaningful dielectric measurements.

A rhombohedral phase corresponding to that of pure $BiFeO_3$ is observed from approximately 75-100 mole percent $BiFeO_3$.

The electrical properties of the solid solutions in the range from 100-50 mole percent $PbZrO_3$ are explained on the basis of a structural model of crystalline $PbZrO_3$ proposed by previous investigators.

ACKNOWLEDGEMENTS

The author wishes to express his sincere gratitude to Drs. William J. James, and Robert Gerson for their guidance and encouragement, and to the faculty of the Department of Ceramic Engineering for their valuable assistance and the use of their equipment. The author is also greatly indebted to Mr. Gary D. Achenbach for his long and earnest assistance through the whole study, and to Mr. James P. Canner, who prepared the hot-pressed ceramics for the microscopic analysis.

The financial assistance of the Atomic Energy Commission in the form of an assistantship is also gratefully acknowledged.

TABLE OF CONTENTS

LIST OF ILLUSTRATIONS

LIST OF TABLES

I. INTRODUCTION

The purpose of this investigation was to analyze the system of lead zirconate, $PbZrO_3$, and bismuth ferrate, $BiFeO_3$, for its phases, structures and lattice parameters.

Until 1961 one of the highest ferroelectric Curie points reported was 490°C for lead titanate, $PbTiO_3$. When $BiFeO_3$ was reported to have a Curie point of approximately 850°C, the possibility of a solid solutions series containing $BiFeO_3$ with a high transition point was suggested. A high Curie temperature is indicative of a pronounced ferroelectric effect. To illustrate this, the following data for ferroelectrics show that the greatest distortion from cubic symmetry occurs for that substance having the highest Curie point.

	Curie Temperature	c/a Ratio
$PbTiO_3$	490°C	1.06
$BaTiO_3$	120°C	1.01
$SrTiO_3$	40°C	1.00

The system of $PbTiO_3$ and $BiFeO_3$ was reported to produce a solid solution with a Curie point above 490°C. The ionic radii of Ti^{+4} (0.64 Å) and Zr^{+4} (0.77 Å) differ by about 17 percent and the ions are isoelectronic with regard to optical electrons.

Therefore, the possibility of solid solutions between $BiFeO_3$ and $PbZrO_3$ exists although some investigators[1][2] have reported being unable to prepare solid solution samples. From a study of the $PbZrO_3$-$BiFeO_3$ system, it should be possible to check the reported high Curie point of $BiFeO_3$ and its purported ferroelectricity.

Since $PbZrO_3$ is known to be an antiferroelectric crystal, it would be of interest to add a ferroelectric such as $BiFeO_3$ and determine if a continuous solid solution were to form. Furthermore, a transition from the antiferroelectric to ferroelectric state would be expected. X-ray and electrical measurements should assist in relating the structural character of the phases and accompanying transitions to a theoretical model.

II. REVIEW OF LITERATURE

A. FERROELECTRICITY AND RELATED PHENOMENA

The phenomenon of ferroelectricity was first discovered by Valsek, while investigating Rochelle salt (sodium potassium tartrate tetrahydrate) in 1921. Such materials were called ferroelectrics because of the analogy of the electrical properties to the magnetic properties of ferromagnetics.[3]

Crystals lacking a center of symmetry may be piezoelectric. A piezoelectric crystal exhibits a displacement of electrical charge upon application of an external strain. A crystal whose center of positive charge does not coincide with its center of negative charge in the absence of an electric field, exhibits a spontaneous polarization which may be altered by a change in temperature. This effect is called pyroelectricity. Ferroelectrics are one class of pyroelectrics, but have the additional property wherein the polarization can be reversed by application of a sufficiently large electric field. In a strong alternating field such crystals show hysteresis effects. Barium titanate has been studied extensively, and was the first dielectric in which the relative displacements of sublattices due to dielectric polarization could be observed by x-ray diffraction (see Figures 1-3). Ferroelectrics have a transition temperature, the Curie above which they are nonpolar and centro-symmetric in structure; they are then described as being paraelectric.

Kittel[4] first stated the theory of antiferroelectricity, and it was first observed for lead zirconate by Shirane[5] and his co-workers in 1951. The distinction between ferroelectricity and antiferroelectricity has been discussed in detail by Kanzig[6] and Megaw,[3] and will be explained later in describing the structure of lead zirconate.

B. PEROVSKITE STRUCTURE

While there exist a large number of ferroelectric structure types, the simplest is the perovskite type. The materials with which we shall be concerned are all perovskites, and we will restrict our discussion to this type of ferroelectric.

The term perovskite is derived from the cubic mineral calcium titanate, $CaTiO_3$. The general structure is shown in Figures 1 and 2 for $BaTiO_3$ but can be generalized for ABO_3. Sub-types of the perovskite family will have the general formula BX_3 ($X = 0^{-2}$ or F^{-1}), and ABX_3. In the ABX_3 structure, A is a large cation, B is a relatively small or middle sized cation with octahedral coordination and X corresponds to 0^{-2}, F^{-1}, Cl^{-1} or Br^{-1}. The major interest now is in the type ABO_3 in which A has a coordination number of 12.

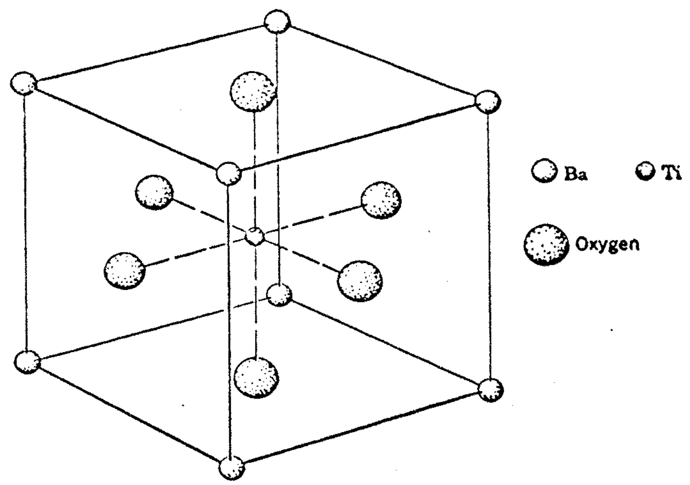

Figure 1. Perovskite crystal structure of barium titanate referred to cubic lattice.[7]

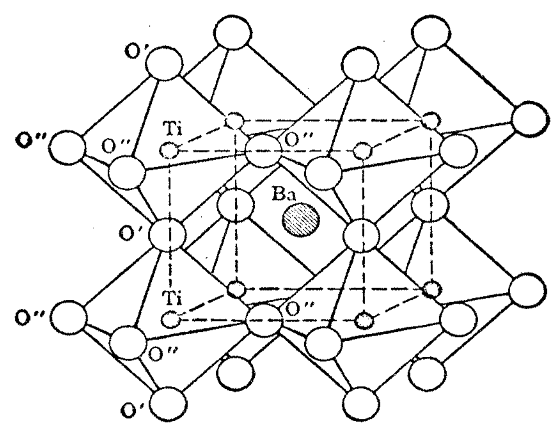

Figure 2. Perovskite crystal structure of barium titanate showing octahedra for oxygen atoms about the titanium atoms.[7]

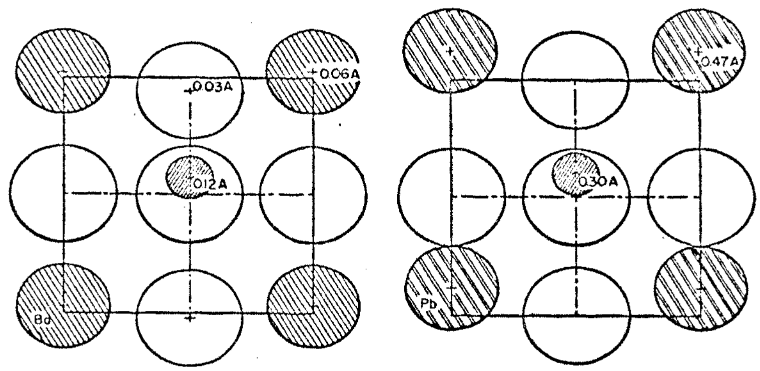

Figure 3. Comparison of the polarization of A and B ions in reference to a rigid oxygen network for $BaTiO_3$ and $PbTiO_3$.[1]

Another way of visualizing the structure of ABO_3 is to look upon it as being built by linear chains of BO_6 octahedra extending along every [100] direction and sharing all corners. These octahedra may or may not be distorted depending on the size and the polarizability of the atoms A and B. Ionic radii and polarizability of some cations are listed in Table I. Additional information relating these properties to the structure is presented in Figures 4-7.

For a perfect fit of the ions into the perovskite structure, the following equation must hold:

$$R_A + R_O = \sqrt{2}\ (R_B + R_O)$$

where

R_A = ionic radius of the large cation

R_B = ionic radius of the smaller cation

R_O = ionic radius of oxygen (= 1.40 Å,[9] 1.32 Å,[10] 1.46 Å[7].)

Since the majority of perovskites do not involve ions which fit this equation exactly, a tolerance factor, t, was introduced by Goldschmidt,[8] where

TABLE 1

Ion	Radius [a]	Polarizability [d]	Ion	Radius [a]
Divalent ions				
	A	A^3		A
Ba^{+2}	1.34	70.6	Mn^{+2}	0.80
Pb^{+2}	1.20	91.8	Fe^{+2}	.74
Eu^{+2}	[b] 1.16	------	Zn^{+2}	.74
Sr^{+2}	1.12	49.1	Co^{+2}	.72
Ca^{+2}	0.99	34.9	Ni^{+2}	.69
Cd^{+2}	.97	• 56.9	Mg^{+2}	.66
			Be^{+2}	.35
Trivalent ions				
Al^{+3}	0.51	------	Bi^{+3}	0.96
Ga^{+3}	.62	------	Gd^{+3}	.97
Cr^{+3}	.63	------	Sm^{+3}	1.00
Fe^{+3}	.64	------	Nd^{+3}	1.04
Sc^{+3}	[c] .80	------	Ce^{+3}	1.07
In^{+3}	[c] .82	------	La^{+3}	1.14
Y^{+3}	.92	------	------	------
Tetravalent ions				
C^{+4}	0.16	------	Sn^{+4}	0.71
Si^{+4}	.42	------	Hf^{+4}	.78
Ge^{+4}	.53	------	Zr^{+4}	.79
Mn^{+4}	.60	------	Ce^{+4}	.94
V^{+4}	.63	------	U^{+4}	.97
Ti^{+4}	.68	------	Th^{+4}	1.02

Radii and polarizability, where used, of metallic ions pertinent to Figures 4, 5, 6 and 7.[8]

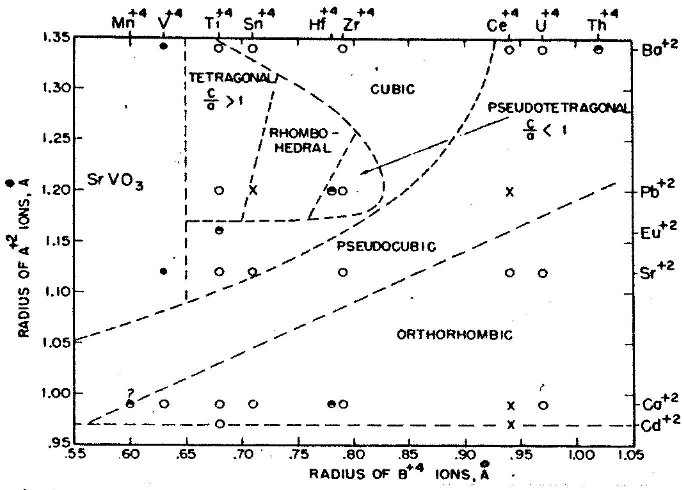

O, Compounds studied in the present work that have the structure shown by the areas bounded by dashed lines; ◓, compounds not studied in the present work that are assumed to have the structure shown by the areas bounded by dashed lines; ●, compounds studied in the present work that do not have the perovskite type structure; X, position of compositions studied in the present work that do not form $A^{+2}B^{+4}O_3$ compounds.

As the compound $CaMnO_3$ has not been studied in the present work and conflicting reports on its symmetry exist, it is tentatively left on the border between orthorhombic and pseudocubic types and is shown by question mark over symbol.

Figure 4. Classification of the perovskite $A^{+2}B^{+4}O_3$-type compounds according to the constituent ionic radii.(8)

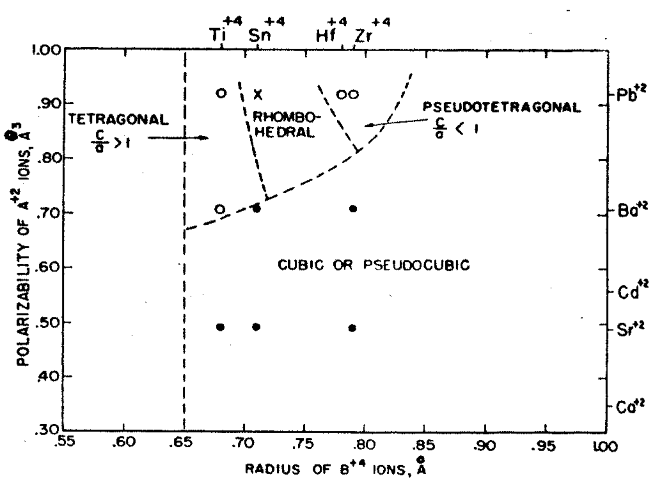

O, Compounds having ferroelectric or antiferroelectric structure types; ● compounds having cubic or pseudocubic structure types; X, position of composition that does not form $A^{+2}B^{+4}O_3$ compound.

Figure 5. Graph of ionic radii of B^{+4} ions and polarizability of A^{+2} ions for some of the compounds of the $A^{+2}B^{+4}O_3$ perovskite structure type.(8)

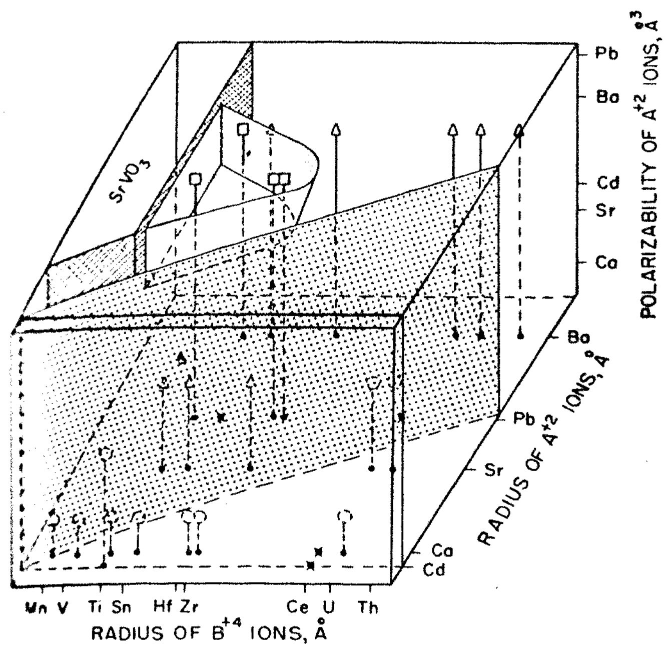

O, Position of compounds of the orthorhombic perovskite structure type; Δ, position of compounds of the cubic or pseudo-cubic perovskite structure type; □, position of compounds having ferroelectric or antiferroelectric perovskite structure types.

Coarse shading indicates boundary between orthorhombic and pseudocubic structure types; medium shading, boundary enclosing compounds of ferroelectric and antiferroelectric structure types; crosshatch shading, boundary between perovskite and $SrVO_3$ structure types. The boundary between cubic and pseudocubic perovskite types has not been shown on this diagram for the sake of clarity.

Figure 6. Three-dimensional graph of the perovskite-type $A^{+2}B^{+4}O_3$ compounds using ionic radii of the A^{+2} and B^{+4} ions as two coordinates and the polarizability of the A^{+2} ions as the third coordinate.(8)

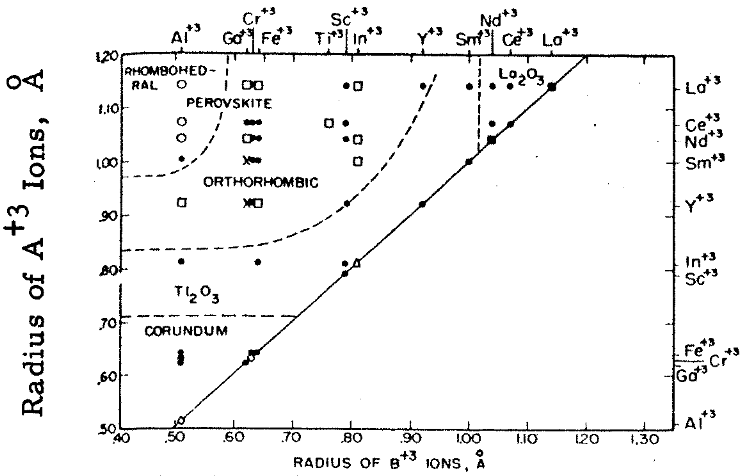

O, Rhombohedral perovskite, $\alpha > 90^{\circ}$; □, orthorhombic perovskite ($CaTiO_3$ type); △, Tl_2O_3 structure type; ◇, corundum structure type; ■, La_2O_3 structure type; ●, compounds not studied in the present work that are assumed to have the structure shown by the areas bounded by dashed lines.

Figure 7. Classification of the $A^{+3}B^{+3}O_3$-type compounds according to the constituent ionic radii.(8)

$$t^{*} = \frac{R_A + R_O}{\sqrt{2}\ (R_B + R_O)}.$$

At room temperature, $SrTiO_3$ has a tolerance factor of 1.0.

If Ba^{++} replaces Sr^{++}, a slight shift of the ions occurs which produces a one percent increase in the parameter, resulting in a tetragonal structure. On the other hand if Ca^{++} replaces Sr^{++}, the structure contracts around the calcium ion, since it is smaller, forming an orthorhombic structure. The substitution of Mg^{++} for Sr^{++} gives an entirely different structure, the ilmenite type, named after the mineral $FeTiO_3$. For a tolerance range of 0.80 to 1.10, the perovskite structure is common. If the tolerance is greater than 1.10 the ilmenite structure is common. The perovskite compounds of the $A^{+2}B^{+4}O_3$ have been assigned a minimum tolerance factor of 0.77 by Keith and Roy.(8) In general for ABX_3 compounds, the change from the perovskite to the ilmenite structure reduces the number of X ions surrounding each A ion from 12 to 6 (see Figure 8). The transition, from perovskite

---

* The radii must be corrected for the coordination number of the ABX_3 perovskite type. For the increased ionic radius resulting from an increase in coordination number from six to twelve, a modified equation is suggested.(11)

$$1.06\ (R_A + R_X) = t\sqrt{2}\ [\,0.95\ (R_B + R_X)\,]$$

where t = the tolerance factor

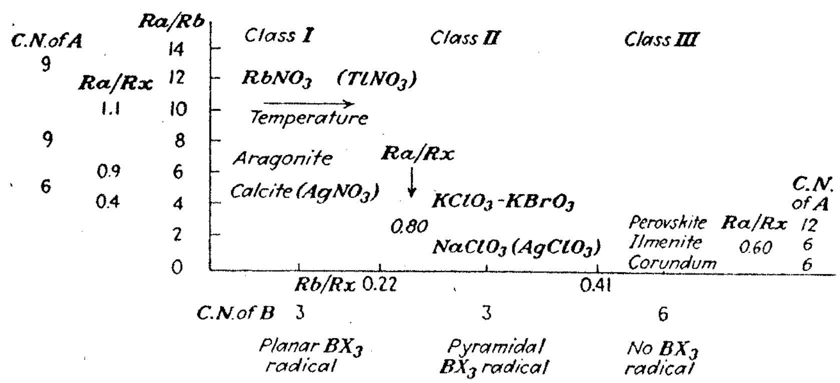

Figure 8. Classification of ABX_3 compounds according to crystal structure.[11]

to ilmenite, should occur when the $R_A:R_X$ ratio falls below 0.73.[11] Ionic radii of Mg^{++}, Ca^{++}, Sr^{++} and Ba^{++} are listed in Table I.

In Figure 6, there is a three-dimensional graph of the perovskite-type A^{+2} and B^{+4} ions as two coordinates and the polarizability of the A^{+2} ions as the third coordinate. As very little is known quantitatively about the polarizability of the trivalent ions in perovskite $A^{+3}B^{+3}O_3$ compounds,[8] this factor has not been used to classify these structures from other $A^{+3}B^{+3}O_3$ compounds. It can be seen from Figure 7 that all of the compounds in the upper left of the diagram having large A^{+3} and B^{+3} ions form perovskite-type structures. No $A^{+3}B^{+3}O_3$ compound is known to have a simple cubic perovskite-type structure.[8] As Bi^{+3} has a radius of 0.96 Å (between Y^{+3} and Sm^{+3}), Figure 7 shows that a possible compounds of $BiFeO_3$ with a perovskite-type structure and low symmetry could be predicted.

Since lead is an important ion in this study, the tolerance factors for Pb^{++} are listed.[12]

	Pb^{++} CN of 6	Pb^{++} CN of 12	Ti^{4+}	Sn^{4+}	Hf^{4+}	Zr^{4+}
Ionic radii (Å)	1.32	1.46	0.64	0.74	0.84	0.87†
Tolerance factor			0.98	0.93	0.89	0.88
Crystal system			tetra.	cubic	tetra.*	ortho.
(volume $Å^3)^{1/3}$			4.00	4.10	4.12	4.13

† This value is quite doubtful. The radius of Zr^{4+} has been reported to be 0.77 Å [10], 0.79 Å [8] and 0.80 Å [9]. If 0.79 Å is used, the tolerance factor of $PbZrO_3$ is 0.92.

* From Kanzig,[6] the structure of $PbHfO_3$ is pseudotetragonal, probably orthorhombic, antiferroelectric, multiple cell.

C. CLASSIFICATION OF PEROVSKITE STRUCTURE

In 1938, Stillwell[11], suggested a method for classifying the ABX_3 compounds according to crystal structure properties, such as $R_a:R_b$ ratio, $R_a:R_x$ ratio, coordination number of A and B, and the structure of the BX_3 radicals. A summary of these properties can be seen from Figure 8. Megaw[3] further classified oxides of the ABO_3 formula as follows in 1957:

1. Cubic perovskite. These have an ideal cubic structure with a cell edge of about 4 Å, one formula-unit per cell, a tolerance factor t = 0.90 - 1.05 and a very simple x-ray pattern. If no other structure exists, these are not ferroelectric.
2. Distorted small-cell perovskite. These are no longer cubic, but with cell edges still approximately 4 Å and t nearly unity, one formula-unit per cell, with each single line of the ideal cubic structure replaced by a group of lines. These substances are ferroelectric.
3. Distorted multiple-cell perovskite. These materials possess a distorted structure in which adjacent units of a 4 Å edge are not perfectly identical, with the true cell made up of a number of these sub-cells. The edges are frequently multiples of a 4 Å with $\sqrt{2}a$ being common. The existence of these multiple cells is recognized by the presence of extra lines on the x-ray powder patterns.

4. Other types, including the ilmenite type. These occur when the factor t falls below a tolerance limit of about 0.75 for compounds where A has a + 1 valency, and which increases with the valency of A. Other structure types, like the La_2O_3, Tl_2O_3, and the $YCrO_3$ types, can also be adapted by ABO_3 compounds with low t values.

The subgroups of the perovskites mentioned above are shown by examples in Table II. Some compounds of the perovskite family are also listed in Table III.

D. $PbZrO_3$, LEAD ZIRCONATE

Lead zirconate was reported by Naray-Szabo(13) in 1943 as a monoclinic type. In 1946, Megaw(14) stated that it was tetragonal with $a_o = 4.1585$ Å and $c_o = 4.108$ Å. Veda and Shirane(3) reported in 1951 that it was tetragonal with a multiple cell; the parameters of the sub-cell are $a_o = 4.150$ Å, $c_o = 4.099$ Å. Sawaguchi(15) and co-workers reported in 1951 that $PbZrO_3$ is actually orthorhombic with the size of the multiple cell approximately $\sqrt{2}\,a_o \times 2\sqrt{2}\,a_o \times 2c_o$, with 8 formula units in the cell. Sawaguchi(16) reported again in 1952 cell parameters of $a = 4.152 \times \sqrt{2} = 5.872$ Å, $b = 4.152 \times 2\sqrt{2} \approx 11.744$ Å, $c = 4.101 \times 2 = 8.202$ Å at 20°C. Jona(17) and co-workers also studied $PbZrO_3$ in 1957 by x-ray and neutron diffraction

TABLE II

I. Substances occurring only in ideal cubic form	$SrTiO_3$, $SrZrO_3$, $SrHfO_3$, $SrSnO_3$, $SrFeO_3$, $BaZrO_3$, $BaHfO_3$, $BaSnO_3$, $BaCeO_3$, $EuTiO_3$, $LaMnO_3$
II. Substances having at least one form with a distorted small-cell structure (C = cubic, T = tetragonal, O = orthorhombic, R = rhombohedral, ? = doubtful or not fully investigated)	$BaTiO_3$ (C, T, O, R), $KNbO_3$ (C, T, O, R), $KTaO_3$ (C, ?), $RbTaO_3$ (C, T), $PbTiO_3$ (C, T)
III. Substances having distorted multiple-cell structures (*a*) cell size $\sqrt{2}a \times 2a \times \sqrt{2}a$ (*b*) cell size $\sqrt{2}a \times 4a \times \sqrt{2}a$ (*c*) cell size $\sqrt{2}a \times 2\sqrt{2}a \times 2a$ (*d*) cell size $2a \times 2a \times a$ (*e*) others	(*a*) $CaTiO_3$, ($CaZrO_3$), ($CdTiO_3$), ($CaSnO_3$) (*b*) $NaNbO_3$, ($NaTaO_3$) (*c*) $PbZrO_3$, $PbHfO_3$ (*d*) WO_3 (*e*) $PbTiO_3$ (low-temp.), WO_3 (high-temp.), $NaNbO_3$ (high temp.), $NaNbO_3$ (low-temp.), $LaCrO_3$
IV. Substances having structures based on close-packing (*a*) Ilmenite type (*b*) $LiNbO_3$ type	(*a*) $FeTiO_3$, $CdTiO_3$ (*b*) $LiNbO_3$, ($LiTaO_3$)

Substances in brackets have not been investigated in detail and classification is partly by analogy.

Classification of substances related to the perovskite structure.[3]

TABLE III

Compounds of the perovskite family.[10]

Compound	Subtype	t	Cell edges	Compound	Subtype	t	Cell edges	Compound	Subtype	t	Cell edges
$CaTiO_3$	d	0,905	7,60	$CaZrO_3$	d	0,854	7,98	$CaThO_3$	d	0,720	8,74
$SrTiO_3$	a	0,982	3,899	$SrZrO_3$	d	0,936	8,19	$SrThO_3$	d	0,789	8,84
$BaTiO_3$	b	1,046	3,986	$BaZrO_3$	a	0,986	4.177	$BaThO_3$	d	0,83_	8,960
			4,026								
$CdTiO_3$	d	0,903	7,50	$CdZrO_3$	d	0,843	—	$CdThO_3$	d	0,711	8,74
$PbTiO_3$	b	1,015	3,89	$PbZrO_3$	c	0,947	8,25	$PbThO_3$	d	0,799	8,95
			4,13				8,34				
$CaCeO_3$	d	0,762	7,70	$CaSnO_3$	d	0,856	7,84				
$SrCeO_3$	d	0,856	8,54	$SrSnO_3$	d	0,950	8,05	$SrHfO_3$	d	0,923	8,138
$BaCeO_3$	d	0,881	8,754	$BaSnO_3$	a	1,001	4,10	$BaPrO_3$	d	0,888	8,708
$CdCeO_3$	d	0,753	7,65	$CdSnO_3$	d	0,855	7,80				
$PbCeO_3$	d	0,846	7,62	$PbSnO_3$	c	0,961	7,86				
							8,13				
$LaAlO_3$	d	1,023	7,58	$LaCrO_3$	a	0,997	3,88	$LaMnO_3$	a	0,997	3,88
$BiAlO_3$	c	1,015	7,61	$BiCrO_3$	c	0,988	7,77				
			7,94				8,03				
$YAlO_3$	d	0,900	7,34	$LaGaO_3$	a	0,997	3,89	$LaFeO_3$	a	0,992	3,89
$CeMgO_3$	d	0,835	8,54	$ThMgO_3$	d	0,864	—				
$NaJO_3$	[illegible]-type			$NaNbO_3$	d	0,858	7,78	$NaTaO_3$	d	0,858	7,76
KJO_3	d	0,960	8,92	$KNbO_3$	a	0,988	4,01	$KTaO_3$	a	0,988	3,98
NH_4JO_3	d	0,996	9,18								
$RbJO_3$	d	1,018	9,04								
$CsJO_3$	d	1,075	9,324								
$KMgF_3$	d	0,945	8,00	$KNiF_3$	d	0,945	8,02	$KZnF_3$	d	0,923	8,10
$CsCdCl_3$	d	0,913	10,40	$CsHgCl_3$	d	0,883	10,88				
$CsCdBr_3$	d	0,905	10,70	$CsHgBr_3$	d	0,879	11,54				

-t: Tolerance factor.

Subtype:

a) Cubic, Z = 1
b) Tetragonal, Z = 1
c) Tetragonal, Z = 8
d) Monoclinic, Z = 8
e) Tetragonal, Z = 16

Z: Number of times the formula quoted is repeated in the unit cell.

to give precise locations for the oxygen ions (see Table IV). The space group was determined to be Pba2. The orthorhombic parameters given by them are: $a = \sqrt{2}\, a_o = 5.884\ \text{Å}$, $b = \sqrt{2}\, a_o = 11.768\ \text{Å}$ and $c = 2c_o = 8.220\ \text{Å}$.

In relationship to the tetragonal cell, this orthorhombic cell can be shown to be a superlattice of size $2a_T \times 2a_T \times 2c_T$, where the subscript T indicates the former tetragonal lattice. Figure 9 shows the antiferroelectric structure inside the orthorhombic superlattice due to antiparallel shifts of the lead atoms along the former cubic [110] direction. Oxygen atoms also suffer antiparallel shifts within the (001) plane, and unbalanced antiparallel shifts along the c direction, these can be seen in Figures 12-15. From Figure 10, a kind of general type of antiparallel displacement is shown. Figures 17 and 18 also show the antiferroelectric properties of $PbZrO_3$. The application of a sufficiently strong electric field will cause a transition from the antiferroelectric to the ferroelectric state. This transition means that the relative position of the atoms inside the cell of $PbZrO_3$ are changed by the applied field. However, this type of transition is valid only for some substances. Above about 230°C, the $PbZrO_3$ phase changes to cubic and is paraelectric (see Figure 11).

According to Jona[17] and his co-workers, the structure of $PbZrO_3$ is centrosymmetric only for the Pb and Zr atoms. The

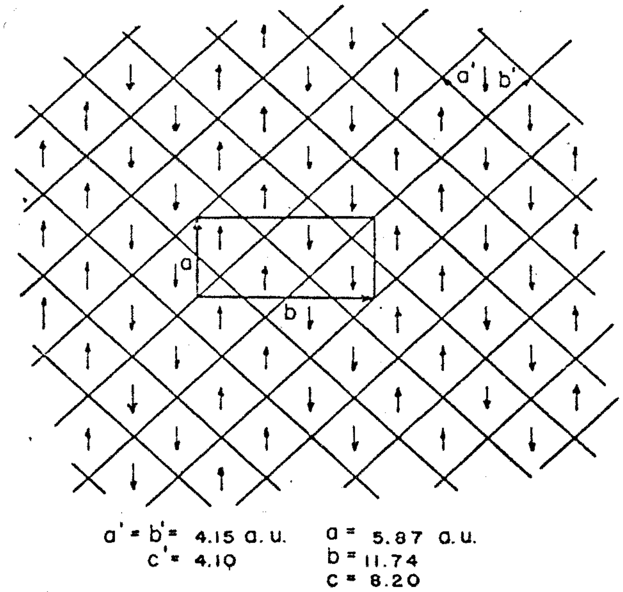

Figure 9. Schematic diagram of the structure of $PbZrO_3$ looking down on the (001) plane of the pseudocubic lattice.[19]

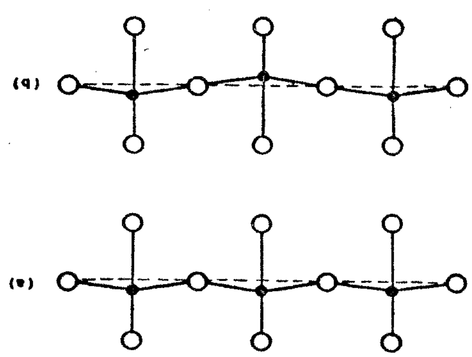

Figure 10. (a) Section through line of octahedra with parallel displacements of central atom.

(b) Section through line of octahedra with antiparallel displacements of central atom.[3]

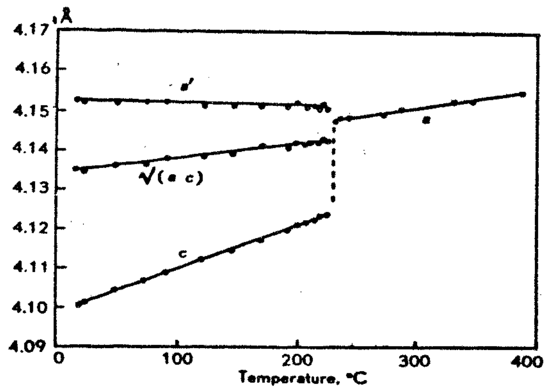

Figure 11. Lattice parameters of the pseudotetragonal cell of $PbZrO_3$ versus temperature.(16)

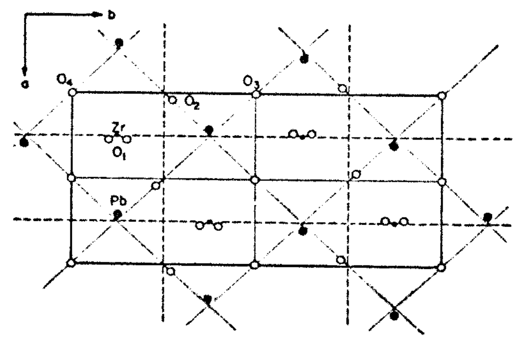

Figure 12. Schematic projection of the room-temperature structure of $PbZrO_3$ on the (001) plane. The dotted lines represent the projection of the original perovskite unit cells. The heavy solid line shows the orthorhombic unit cell. The dashed lines show the traces of the glide planes.(17)

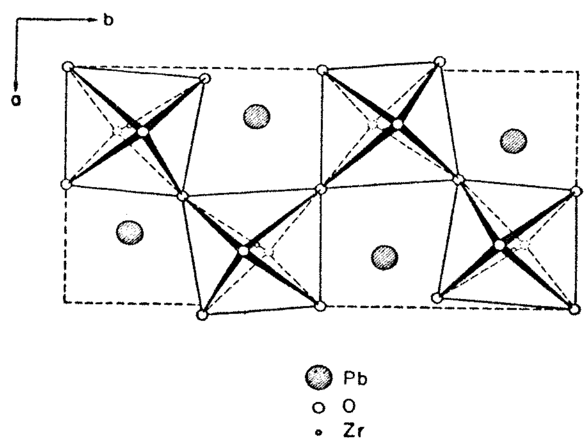

Figure 13. Schematic view of one layer of ZrO_6 octahedra of $PbZrO_3$ as seen along [001] direction.(17)

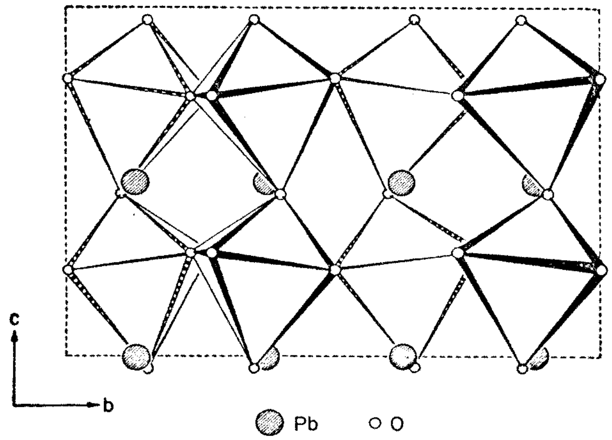

Figure 14. Schematic view of ZrO_6 octahedra network of $PbZrO_3$ as seen along [100] direction. (17)

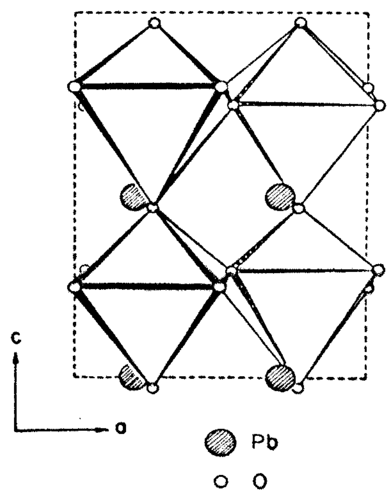

Figure 15. Schematic view of ZrO_6 octahedra network of $PbZrO_3$ as seen along [010] direction. (17)

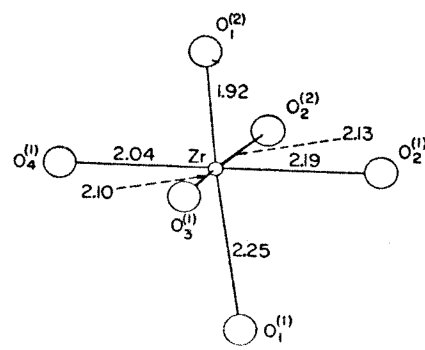

Figure 16. Environment of Zr in $PbZrO_3$. Interatomic distance are given in Å. (17)

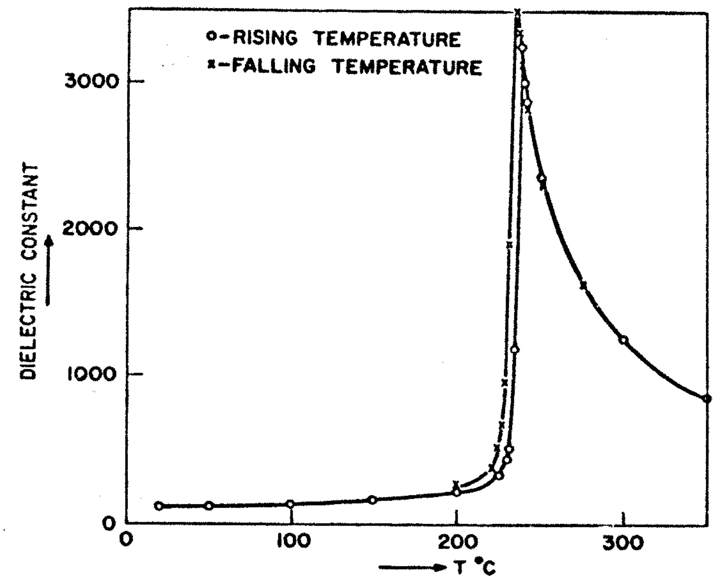

Figure 17. Dielectric constant of polycrystalline $PbZrO_3$ versus temperature.[18]

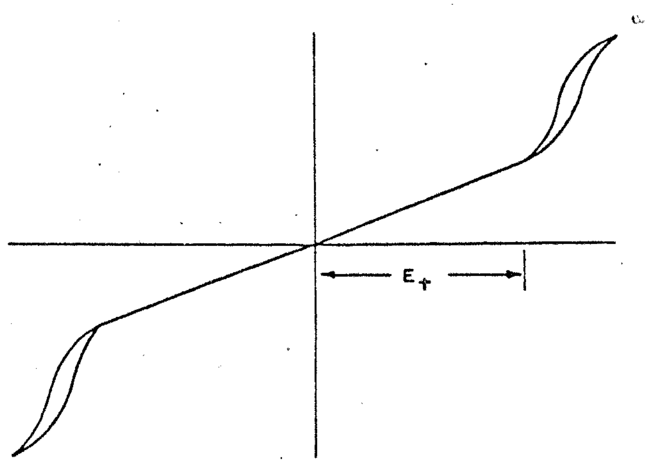

Figure 18. Hysteresis loop of $PbZrO_3$ obtained at a temperature slightly below the transition with moderately high field strength.[19]

noncentrosymmetry is due to shifts of oxygen atoms as revealed by neutron diffraction analysis. This is in accord with the presence of a small piezoelectric effect as cited by Roberts.[18] The oxygen octahedra surrounding the Zr atoms appear to be distorted, and it is possible to explain the strong optical anisotropy within the (001) plane as well as the equality b = 2a. The reasons for these two properties can be illustrated by Figure 12. An expansion is expected in the a direction, along which the Pb atoms are displaced antiparallel to each other, and the oxygens O_1 and O_2 are also found to be displaced in the b direction, thus equalizing the parameters along the orthorhombic a and b axis.

As seen from Figures 12-15, it is clear that $PbZrO_3$ is not an antiferroelectric in the sense first introduced, theoretically, by Kittel.[4] Kittel's hypothetical crystal involves two or more sublattices with equal and opposite polarizations, so that the resulting structure is centrosymmetric. Accordingly no piezoelectric effect should be detected, but the facts cited in the last paragraph show that the structure of $PbZrO_3$ does not follow this description. $PbZrO_3$ is antiferroelectric only in the ab plane, since all the atoms shifts within this plane are antiparallel; but it is definitely polar along the c direction because of the unbalanced shifts of oxygen atoms in this direction (see Table IV). $PbZrO_3$ is believed to be non-ferroelectric along the [001] direction, as the reversal

TABLE IV

	x	y	z	Perovskite coordinates			Shift (Å)
4 Pb in 4(c)	0·706	0·127	0·000	$\frac{3}{4}$	$\frac{1}{8}$	0	0·26
4 Pb′ in 4(c)	0·706	0·127	0·500	$\frac{3}{4}$	$\frac{1}{8}$	$\frac{1}{2}$	0·26
4 Zr in 4(c)	0·243	0·124	0·250	$\frac{1}{4}$	$\frac{1}{8}$	$\frac{1}{4}$	0·04
4 Zr′ in 4(c)	0·243	0·124	[0·750]	$\frac{1}{4}$	$\frac{1}{8}$	$\frac{3}{4}$	0·04
4 O_1 in 4(c)	0·270	0·150	0·980	$\frac{1}{4}$	$\frac{1}{8}$	0	0·35
4 O_1' in 4(c)	0·270	0·100	0·480	$\frac{1}{4}$	$\frac{1}{8}$	$\frac{1}{2}$	0·35
4 O_2 in 4(c)	0·040	0·270	0·300	0	$\frac{1}{4}$	$\frac{1}{4}$	0·53
4 O_2' in 4(c)	0·040	0·270	0·750	0	$\frac{1}{4}$	$\frac{3}{4}$	0·34
2 O_3 in 2(b)	0	$\frac{1}{2}$	0·250	0	$\frac{1}{2}$	$\frac{1}{4}$	0·00
2 O_3' in 2(b)	0	$\frac{1}{2}$	0·800	0	$\frac{1}{2}$	$\frac{3}{4}$	0·41
2 O_4 in 2(a)	0	0	0·250	0	0	$\frac{1}{4}$	0·00
2 O_4' in 2(a)	0	0	0·800	0	0	$\frac{3}{4}$	0·41

Interatomic distances

Range of Zr—O distances: 1·92—2·25 Å.

Shortest Pb—O distances: 2·53, 2·58, 2·58 Å.

Atomic positions in the unit cell of $PbZrO_3$. The corresponding coordinates in the ideal perovskite structure, and the amounts of shift from these positions are given in the last two columns. [17]

of the c axis involves an opposite distortion of the oxygen octahedra, and the reversal of the polarization of the Pb sublattices within the (001) plane. It is conceivable that the amount of energy necessary for such a reversal is very large, and the crystal prefers to assume, under a strong electric field, and very near to the transition temperature, a completely different type of structure with ferroelectric properties. [17]

Figure 16 shows the environment of Zr in $PbZrO_3$. Calculated intensities contributed by oxygen atoms of $PbZrO_3$ at room temperature structure can be seen in Table V from neutron diffraction analysis. [17]

The $PbZrO_3$ - $PbTiO_3$ system has been reported by Shirane, Suzuki and Takeda[20] in 1952 and Sawaguchi[21] in 1953 to have orthorhombic, rhombohedral and tetragonal phase regions as shown in Figure 19. In Figure 20 a diagram of Curie temperature as a function of composition is presented. F_α and F_β are ferroelectric, A_α represents an antiferroelectric and P_α the paraelectric. The Curie temperature increases nearly linearly as the proportion of $PbTiO_3$ is increased. Figure 20 shows that a structure change from orthorhombic on the $PbZrO_3$ side to rhombohedral causes a transition from antiferroelectric to ferroelectric. The system near 100% $PbZrO_3$ is a multiple cell orthorhombic phase with antiferroelectric properties.

TABLE V

Comparison between observed and calculated intensities of neutron powder diffraction lines of $PbZrO_3$.(17)

Line number	*hkl*	Observed intensities, in counts/min (a) First run	(b) Second run	Calculated intensities Final model	Oxygen unshifted	All atoms unshifted
0*a*	110	203	190	223	70	0
1	120 002	301	293	291	171	150
1*a*	130 112	256	249	256	117	0
2	200 040 122 210	2672	2746	2681	2450	2556
3*a*	132 221 141 023	731	718	588	0	0
3	113 202 042 230 212	2955	3097	3575	4861	4985
4	151 to 241	5811	5640	5531	6712	7048
4*a*	213 to 143	653	a	616	112	0
5	311 to 321	544	a	452	341	119
5*a*	251 to 134	528	a	505	275	0
6	153 to 243	2717	a	3010	1504	1716
6*a*	260 to 115	515	a	691	178	0
8	262 to 045	4509	a	4539	6644	6995
9	180 to 361	1891	a	1758	917	83
10	334 to 273	1016	a	952	742	1013
$R = (\Sigma \lvert I_{calc} - I_{obs} \rvert)/\Sigma I_{obs}$ for all lines up to angle $2\theta = 54°$				0.07	0.44	0.54

a Not recorded.

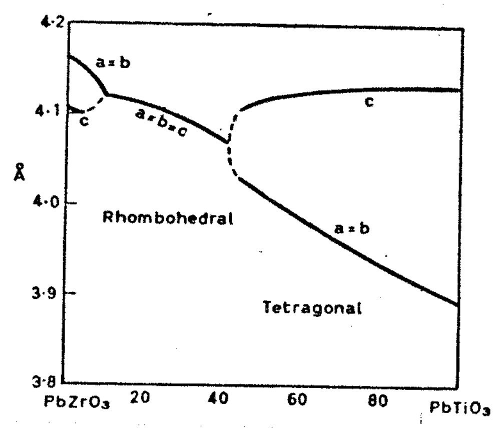

Figure 19. Lattice dimensions of the solid solution series between $PbTiO_3$ and $PbZrO_3$ at room temperature.[20]

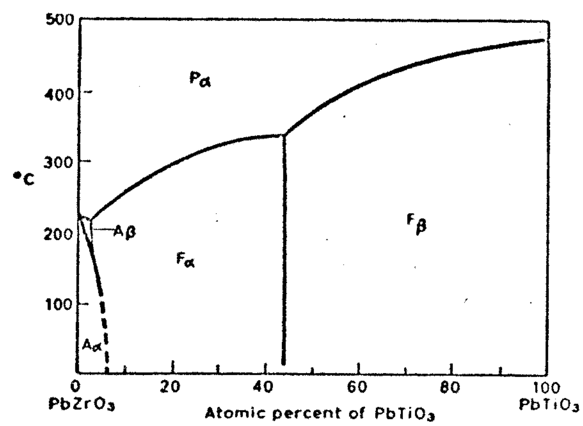

Figure 20. Phase diagram of the solid solution series between $PbTiO_3$ and $PbZrO_3$. A, F, P denote antiferroelectric, ferroelectric, and paraelectric, respectively.[21]

E. $BiFeO_3$, BISMUTH FERRATE

The system Bi_2O_3-Fe_2O_3 was studied in 1957 by Royen and Swars[22] from 0 to 55 mole percent Fe_2O_3 in Bi_2O_3 in the temperature range 650-1100°C. Several phases were found and identified as:

1. $20Bi_2O_3 \cdot Fe_2O_3$ crystallizing at 835°C is tetragonal.
2. (12-13) $Bi_2O_3 \cdot Fe_2O_3$ crystallizing from melts at 790-810°C, is tetragonal.
3. Below 765°C, the compounds mentioned in 1 and 2 decompose. The compound $15Bi_2O_3 \cdot Fe_2O_3$, with a limited solid solution range, forms at this temperature in a body-centered cubic structure.
4. $Bi_2O_3 \cdot Fe_2O_3$ obtained at 935°C, is tetragonal, with $a = 11.91 \pm 1$ Å, $c = 13.73 \pm 1$ Å.
5. Below 825°C, $2Bi_2O_3 \cdot Fe_2O_3$ forms in a tetragonal structure, $a = 12.102 \pm 7$ Å, $C = 17.865 \pm 8$ Å.

Filip'ev[23] and co-workers in 1960, Fedulov[24] and co-workers in 1961, and Zaslavskii and Tutov[25] in 1962 have reported the structure of bismuth ferrate as a rhombohedral distorted perovskite with parameters $a = 3.957 \pm 0.001$ KX, $\alpha = 89°28' \pm 2'$; $a = 3.963$ Å, $\alpha = 89°24'$ and $a = 3.952 \pm 0.001$ KX, $\alpha = 89°36' \pm 3'$ respectively. This structure has a tolerance factor of 0.89,[25] with three formula units per hexagonal cell. The relation between the rhombohedral and hexagonal phases is shown in Figure 21.

Filip'ev[23] reported the samples were prepared from mixtures of Bi_2O_3 and Fe_2O_3 by double firing at 800°C for 1 hour. The products were found to be single phase within the accuracy of his photographic method. Figure 22 shows that the rhombohedral unit cell parameter, a, varies linearly with temperature from 3.96 Å at 0°C to 4.00 Å at 800°C. The rhombohedral angle is constant over this temperature range.

Filip'ev found the compound starts to form at 600°C and begins to dissociate to Bi_2O_3 and Fe_2O_3 above 725°C. Fedulov reports that decomposition starts at 700°C, and at 800°C the dissociation is extensive. The decomposition is not reversible. Crystals of $BiFeO_3$ grow rapidly at 850°C and can be isolated up to one millimeter in size from excess Fe_2O_3 by using concentrated nitric acid. The x-ray density of $BiFeO_3$ is 8.37 g/cm^3; this differs from the directly measured density by less than 3% as stated by Filip'ev.

Differential thermal analysis of $BiFeO_3$, shows in Figure 23 that no phase transition occurs below about 850°C, but endothermic changes occur at 875-930°C, 970-1030°C, and 1030-1090°C, accompanied by substantial shrinkage, which is believed by Fedulov[24] to result from the incongruent melting of the $BiFeO_3$. From these

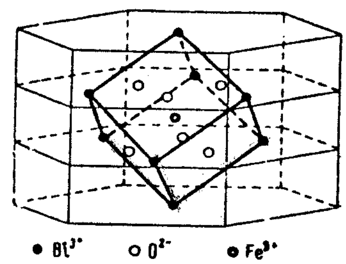

Figure 21. Relationship of the rhombohedral unit cell to the hexagonal for $BiFeO_3$.[25]

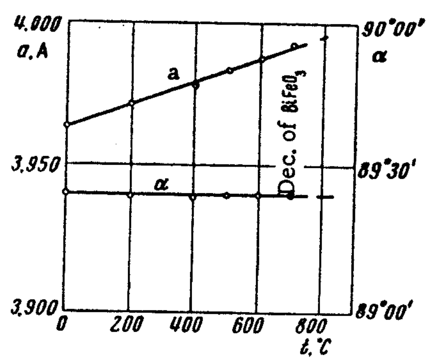

Figure 22. Results for a and α of the rhombohedral unit cell of $BiFeO_3$ as functions of temperature.[24]

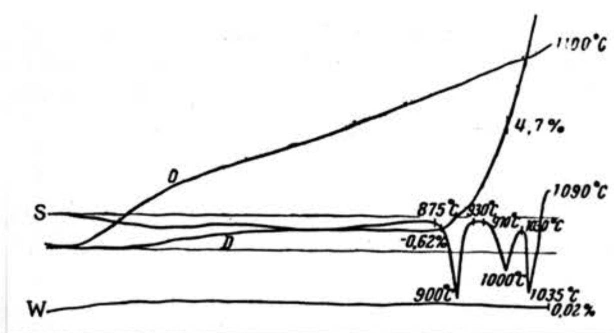

Figure 23. Thermal-analysis curves for $BiFeO_3$. D = d. t. a., S = shrinkage, W = weight loss, and O = temperature of specimen.[24]

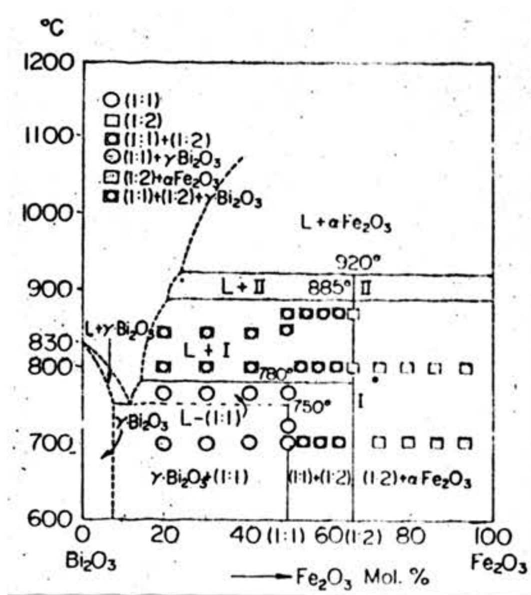

Figure 24. Phase diagram for the Bi_2O_3-Fe_2O_3 system (various symbols indicate the results of x-ray diffraction analysis).[27]

results, the Curie point for $BiFeO_3$ should lie above 850°C, making it useful for the possible preparation of solid solutions with a high Curie temperature. Fedulov(26) has estimated this temperature to be approximately 850°C, which is very high compared to other known ferroelectrics.

Ceramic samples of the Bi_2O_3-Fe_2O_3 system were investigated by Koizumi, Niizeki and Ikeda(27) in 1964, as seen in Figure 24. Two intermediate binary phases, a $Bi_2O_3 \cdot Fe_2O_3$ compound, and a $Bi_2O_3 \cdot 2Fe_2O_3$ compound, occur in this system. $BiFeO_3$ was identified to be a pseudo-cubic rhombohedral perovskite, and $Bi_2Fe_4O_9$ was reported as an orthorhombic crystal structure with lattice constants, a = 7.97 ± 0.01 Å, b = 8.43 ± 0.01 Å, and c = 6.01 ± 0.01 Å. Detailed indices are given in Appendix ~~B~~ C.

F. SOLID SOLUTIONS OF $BiFeO_3$

Since $BiFeO_3$ does not reveal a ferroelectric phase transition up to its incongruent melting point (~850°C), the possibility of high Curie points for its solid solutions is of great interest. As $BiFeO_3$ is a substance with both magnetic(28) and ferroelectric properties, the study of $BiFeO_3$ and its solid solutions is of interest for determining the possibility of preparing materials having magnetic and ferroelectric properties simultaneously.

The $BiFeO_3$-$PbTiO_3$ system was first reported by Fedulov(26)(29) and his co-workers in 1962 and 1964. This system is shown in Figures 25-27. A narrow two phase region, with tetragonal and rhombohedral modifications was observed from 65.3 to 72.4 wt. % $BiFeO_3$. The rhombohedral angle is nearly constant through the rhombohedral phase region. As $PbTiO_3$ is added to the pure $BiFeO_3$, the Curie point decreases as the crystal stability increases. From Figure 27, the Curie point of pure $BiFeO_3$ was estimated by extrapolation to be 850^oC. The data used in this figure were obtained from magnetic measurements and x-ray analysis, which permitted construction of the detailed phase diagram of the solid solutions of the $PbTiO_3$-$BiFeO_3$ system.

Roginskaya[30] and co-workers investigated the system $BiFeO_3$-$LaFeO_3$ in 1963, in which $LaFeO_3$ is a noncollinear antiferromagnet (weak ferromagnet) with the perovskite structure. X-ray data in Figures 28 and 29 show that over the entire range of concentrations a continuous series of solid solution exists with a distorted perovskite cell up to 18.8 mole % $LaFeO_3$ in the rhombohedral modification, from 18.8 to 55 mole % $LaFeO_3$ in the pseudo-monoclinic I (PM-I), from 55 to 73 mole %$LaFeO_3$ in the pseudo-monoclinic II (PM-II), higher, 75 mole % $LaFeO_3$ in the pseudo-monoclinic modification III (PM-III). The character of the splitting of the main lines in the PM-I region corresponds to a tetragonal distortion of the cell with $c/a < 1$. However, the superlattice lines observed on the x-ray patterns of specimens in this region show

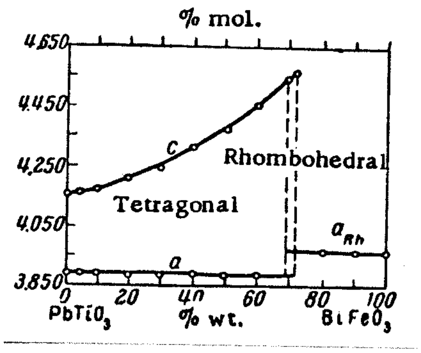

Figure 25. Change in the lattice parameters in a system of solid solutions of $PbTiO_3$-$BiFeO_3$ as a function of the composition.(26)

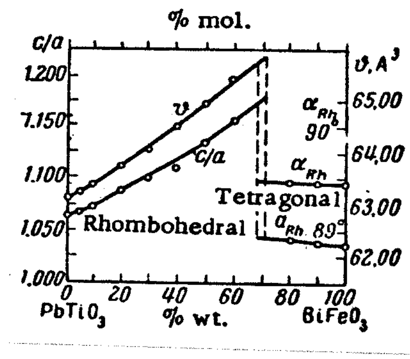

Figure 26. The volume and axial ratio c/a of the unit cells of solid solutions in the $PbTiO_3$-$BiFeO_3$ system versus the composition.(26)

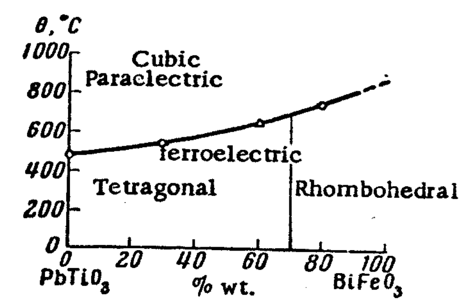

Figure 27. Phase diagram of the system $PbTiO_3$-$BiFeO_3$.(26)

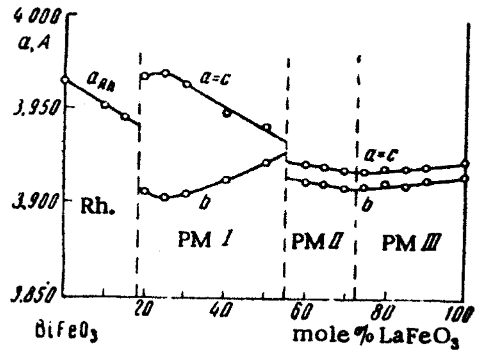

Figure 28. Dependence of the unit cell parameters of various modifications of solid solutions of (Bi, La) FeO_3 on the composition.(30)

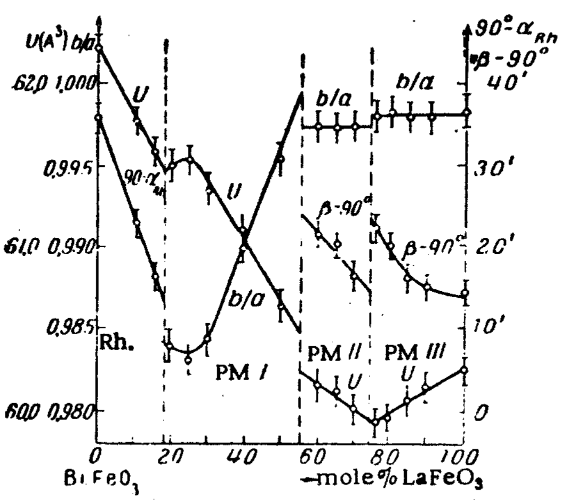

Figure 29. Dependence of the unit cell parameters on the composition in various modifications of solid solutions of (Bi,La)FeO_3.(30)

this modification to be similar to the compound $PbZrO_3$, with antiferroelectric properties.

Krainik[31] and co-workers, and Zhdanova[32] reported simultaneously in 1965 on their work with the $BiFeO_3$-$PbFe_{1/2}Nb_{1/2}O_3$ system. Krainik's description is shown in Figure 30. The x-ray analysis shows, within the precision of the measurements, a cubic phase from 5-60 mole % $BiFeO_3$ and a rhombohedral phase from 70-100%. Krainik mentioned in his paper that Buhrer[33] reported superstructure lines in the rhombohedral phase and that these solutions do not possess ferroelectric properties. But Krainik reports he found no reliable lines indicating a complication of the unit cell in the rhombohedral phase. In certain samples of the system a small amount of the impurity $Bi_2O_3 \cdot 2Fe_2O_3$ was found.[34] Zhdanova's results are shown in Figure 31. He stated that adjacent to $PbFe_{1/2}Nb_{1/2}O_3$, solid solution exists with a pseudocubic structure, and adjacent to $BiFeO_3$, solid solution with a rhombohedral structure exists. A broad morphotropic boundary evidently passes through the system near 65 mole % $BiFeO_3$. In Figure 31, (H) 1 and (H) 2 are the temperatures of the first and second phase transitions, respectively.

It has been established by Roginskaya and Venevtsev[35] in 1965 that in the system of $BiFeO_3$-$LaCrO_3$ a continuous series of solid solution forms, consisting at room temperature of four modifications (one rhombohedral and three pseudomonoclinic, i.e., PMI, PMII and PM III) as seen in Figure 32. All of the solid solutions are antiferromagnetic with weak ferromagnetism. The phase diagram of this system is similar to that shown in Figure 28.

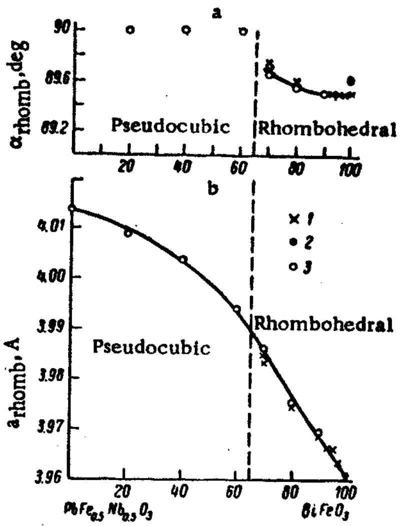

Mole percent of $BiFeO_3$

Figure 30. Composition dependence of the lattice parameters α_{rhomb} and a_{rhomb} of the unit cell in solid solutions of the $BiFeO_3$-$PbFe_{1/2}Nb_{1/2}O_3$ system. (31)

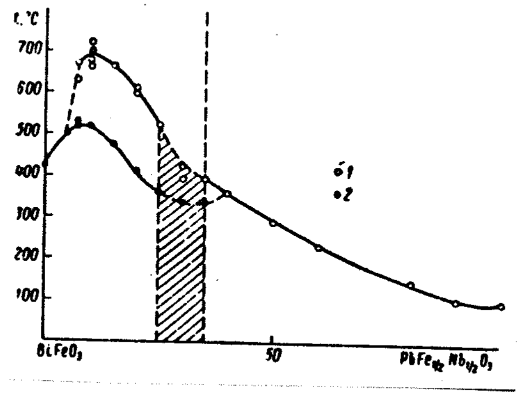

Mole percent of composition

1) (H) I. 2) (H) II.

Figure 31. Phase-transformation temperature as a function of composition in the $BiFeO_3$-$PbFe_{1/2}Nb_{1/2}O_3$ system. (32)

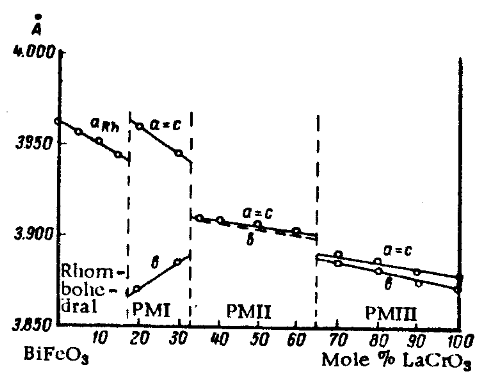

Figure 32. Dependence of the parameters of the unit cells of the solid solutions on composition in the system $BiFeO_3$-$LaCrO_3$.(35)

III. EXPERIMENTAL PROCEDURE

A. SPECIMEN PREPARATION FOR THE $PbZrO_3$-$BiFeO_3$ SERIES

The starting chemicals were reagent grade lead monoxide, PbO; zirconium oxide, ZrO_2; bismuth trioxide, Bi_2O_3; and technical grade iron oxide, Fe_2O_3.

In this series, compositions were arbitrarily selected at five or ten mole percent intervals between 100 percent lead zirconate and 100 percent bismuth ferrate. After weighing the reagents on an analytical balance with an accuracy to 1/10000 gram, the powders were mixed in an agate mortar and pestle for approximately 15 minutes. Most of these mixtures were then dry mixed using an automatic mortar and pestle for 4 hours, and a few were ground by hand for 1.5 to 2 hrs. Some of the mixtures of 100 percent $BiFeO_3$ composition were then pressed in a 0.375 inch pill die at 15000 psi to form discs of 0.080 to 0.100 inch thickness. Others were pressed into discs by hand in the same die.

These mixed powders or discs were sintered. Samples for microscopic analysis were prepared by taking a part of the sintered products and hot pressing it into discs using a 3/4 inch die at 10000-25000 psi at temperatures from 700-870°C. Both hot pressing and density measurements of some of these discs were performed by Mr. James P. Canner in the Department of Physics (see Table VII).

X-ray pure samples of $BiFeO_3$ were prepared by adding an excess of Bi_2O_3 (1.5-2.0 mole Bi_2O_3:1.0 mole Fe_2O_3). The mixed specimens were sintered at 800°C for 2 hours and air quenched. The sintered samples were then ground to fine powders, and excess Bi_2O_3 was leached out with warm concentrated nitric acid. The leaching lasted only about ~~15 to 25~~ 10 ~~secon~~ds minutes as $BiFeO_3$ is slightly soluble in the warm concentrated nitric acid. After leaching, the acid was decanted from the sample and the leaching repeated twice to completely remove all ~~Bi_2O_3~~ Bi^{+} in HNO_3 from the residue. Then the residue was rinsed with distilled water several times. The repeated acid leaching is required, in part, to avoid hydrolysis, i.e., formation of a white colloid, $BiO(NO_2)$, when water is added to rinse the residue. If some dissolved Bi_2O_3 remains in the residue, hydrolysis will occur when water is added. This work was done cooperatively with Mr. Charles T. Shih.

B. SINTERING PROCEDURE

After the samples were all mixed or formed into discs, they were placed in covered platinum-lined alumina (marganite) crucibles about 0.6 inch in diameter and 3/4 inch in height.

Sintering was accomplished in an electrical platinum resistance-furnace with an automatic temperature control. The temperature scale of this furnace was calibrated twice by a chromel alumel thermocouple and a compact portable potentiometer. The temperature, time and other sintering conditions for the individual firings are given in Appendix A. Some of the sintered samples were air or water quenched after sintering. A few samples were weighed before and after sintering.

C. X-RAY DIFFRACTION ANALYSIS

Each sintered sample was reground into a fine powder and then analyzed on one or more of the following x-ray diffractometers.

1. Norelco Diffractometer, Type No. 42322. The 2θ range is 0^{o}-90^{o} with rates of 1 or 2 degrees per minute. The rate of 2^{o}/min was used frequently as the driving motor for the other rate was out of order. Only one direction, i.e., decreasing 2θ, is possible on this diffractometer.

2. Norelco Diffractometer, Type No. 12045 B/3. The 2θ range is 0^{o}-180^{o} and drive rates are 2^{o}, 1^{o}, $1/2^{o}$, $1/4^{o}$ or $1/8^{o}$ per minute. 2θ can be driven from both directions. X-ray analyses data listed in Table VI and Appendix C are taken primarily from this unit at a rate of 1^{o}/min and a 2θ range of 10^{o}-95^{o}. Lower rates of this unit were employed for resolving some particular peaks, especially the main peaks of the rhombohedral phases of the $PbZrO_3$-$BiFeO_3$ system.

3. General Electric Diffractometer, Model BR, Type 1. The 2θ range is from -10°-180° with rates of 2°/min or 0.2°/min. Samples of the 100, 75, 50, 25 and 5 mole percent $PbZrO_3$ of the $PbZrO_3$-$BiFeO_3$ system were examined by this unit at a rate of 2°/min and a 2θ range about 10°-98°.

4. Siemens Diffractometer, Type No. U8-006. The 2θ range is 0°-180° at rates of 1°/min and 0.1°/min. Examinations of preparations of pure $BiFeO_3$ and 60-50 mole percent $PbZrO_3$ samples of the $PbZrO_3$-$BiFeO_3$ system were performed on this unit.

For the two Norelco Diffractometers, alignment was calibrated frequently by using a standard quartz sample.

Most of the samples were examined using Cu $K\alpha$ radiation except for a few where iron $K\alpha$ radiation was employed to reduce fluorescence. The IBM 1620 digital computer, located in the UMR Computer Science Center, was used to calculate the values of the lattice parameters.

D. PREPARATION OF POLISHED SAMPLES

Some of the hot-pressed discs described previously were mounted in bakelite and then ground on 400 and 600 grit, Automat abrasive paper. They were polished again on a Buehler low-nap

Metcloth with alumina-A abrasive. After polishing, the samples were x-rayed, and then etched by dipping into a solution of 1 percent HNO_3, 1 percent HF, and 98 percent (b. w.) distilled water for 1/3 to 5 seconds followed immediately by a rinse with tap water. Only one sample was etched in a solution of 1 percent HNO_3, 1 percent HCl, and 98 percent (b. w.) distilled water for 30 minutes. These samples were used for microscopic analysis. Conditions for hot pressing these samples are listed in Table VII.

E. MICROSCOPIC EXAMINATION

The polished samples were examined and photographed at 500-1000X using both polarized (crossed nicols) and unpolarized light before and after etching, on a Bausch and Lomb research metallograph located at the Department of Metallurgical Engineering.

IV. EXPERIMENTAL RESULTS AND DISCUSSION

A. SINTERING

The determination of the time and temperature of sintering the mixed oxides for preparing 100 percent $PbZrO_3$ and $BiFeO_3$, especially for the latter, was a trial process as shown by the data presented in Appendix A. For the other compositions of the $PbZrO_3$-$BiFeO_3$ system, the time and temperature of sintering were kept constant at 2 hours and 870°C. This temperature is quite close to the melting point of bismuth ~~tri~~sesquioxide, Bi_2O_3, (860°[36]). The firing temperatures indicated in Appendix A vary $\pm$ 8°C because the temperature of the automatically controlled furnace has a fluctuation about the set temperature.

The sintered samples were usually air quenched in an attempt to get single phase products. The results of air quenching are given in the next section.

The furance was usually closed during sintering. In a closed system, decomposition and evaporation of the oxides may then be minimized. For example, Fe_2O_3 will be decomposed to a small extent as indicated by the following reaction,

$$6Fe_2O_3 \rightarrow 4Fe_3O_4 + O_2 \uparrow .$$

At 1200°C, the partial pressure of oxygen of this reaction is of the order of 10^{-4} atm.[37] For the $PbZrO_3$-$BiFeO_3$ system, the sintered samples in a closed system usually showed smaller amounts of foreign phases on the x-ray patterns, than for samples prepared in an open system. The effect was, however, quite small. In general, sintered samples prepared in a closed system and quenched in air give relatively clean and well-defined x-ray patterns. X-ray data listed in Table VI are taken on samples prepared under these conditions. After firing, a yellow colored layer was present inside the crucible. This color indicated evaporation of PbO or Bi_2O_3 or both. After sintering a sample of 90.47 mole percent $PbZrO_3$-9.53 mole percent $BiFeO_3$ at 870°C in a closed system, the weight loss was found to be about 3 mole percent. If the weight loss were attributed solely to evaporation of PbO, this corresponds to about 4.5 mole percent of PbO. X-ray patterns of this sample exhibited peaks of ZrO_2. The amount percent was estimated to be about 5 mole percent. This estimation was made by mixing different amounts of ZrO_2 powder to the 90.47 mole percent $PbZrO_3$ sample and to pure $PbZrO_3$, and then examining the intensity change of their x-ray patterns. This result also proves that some evaporation of PbO occurs during sintering of some samples in the $PbZrO_3$-$BiFeO_3$ system.

During one investigation a sample of 42.85 mole percent $PbZrO_3$ was melted extensively by sintering at 1200°C.

The color of $PbZrO_3$ is light cream. As $BiFeO_3$ content is increased in the samples of the $PbZrO_3$-$BiFeO_3$ system, the color of the powders changes gradually from cream (95 mole percent $PbZrO_3$) to dark brown (5 mole percent $PbZrO_3$). The hardness and volume shrinkage of this sintered disc generally increases as the $BiFeO_3$ composition is increased. Hot-pressed samples as listed in Table VII show the same effect. However, these properties can only be regarded as relative since no accurate measurements of hardness and volume shrinkage for the system were made.

For the preparation of 100 percent $BiFeO_3$, mixtures of equimolar Bi_2O_3 and Fe_2O_3 were sintered at 725-850°C, but the samples were always multiphase. However, x-ray pure $BiFeO_3$ samples were made by adding excess Bi_2O_3, sintering at 800°C, followed by leaching with HNO_3 (see page 41). Two samples of equimolar mixtures of Bi_2O_3 and Fe_2O_3, were pressed into discs at 15000 psi and then sintered at 850°C. One of these two sintered discs was cooled slowly after firing. The amount of $Bi_2O_3 \cdot 2Fe_2O_3$ present was larger than found in other samples sintered from the same equimolar mixtures. This may be explained in two ways. First, the sintering temperature of 850°C is higher than in the other cases and therefore dissociation of $BiFeO_3$ will be greater. Furthermore rapid quenching usually produces more of the desired phase.

Double firing at suitable temperatures and sintering periods as well as other sintering techniques may also be used to prepare samples of higher purity.

B. X-RAY DIFFRACTION ANALYSIS

Within the firing temperature range 870°-1200°C, 100 percent $PbZrO_3$ samples were made by sintering equimolar mixtures of PbO and ZrO_2. X-ray patterns of these samples show no obvious difference, except that the air quenched sample has the (131) line ($2\theta = 29.10$, $I/I_o = 4$) appearing with a higher intensity. These samples, as verified by x-ray powder diffraction analysis, are pure $PbZrO_3$ with an orthorhombic multiple cell, containing eight formula-units and dimensions of approximately $\sqrt{2}\, a_o \times 2\sqrt{2}\, a_o \times 2\, c_o$ (see page 16), here a_o and c_o represent the tetragonal parameters. This result is in good accordance with Sawaguchi's lattice constants[16] and indexing for pure $PbZrO_3$ as given in Appendix C. This structure can also be indexed as pseudo-tetragonal. However, the distinction from a real tetragonal structure is the appearance of superlattice lines such as (110), (112), etc. Variations of the mole ratio of the PbO and ZrO_2 mixture from 1:1 were made from 15 mole percent excess PbO to 10 mole percent excess ZrO_2. X-ray analyses of these fired samples show the main products are still $PbZrO_3$, with the excess phase of PbO or ZrO_2 present.

In the $PbZrO_3$-$BiFeO_3$ system, the orthorhombic multiple cell with parameters a, b and c corresponding approximately to $\sqrt{2}\, a_o$, $2\sqrt{2}\, a_o$ and $2\, c_o$ respectively exists from 100 to approximately

30 mole percent $PbZrO_3$. The parameters decrease slightly and continuously in the range 100-80 mole percent $PbZrO_3$, except that c increases a little from 85 to 81.81 mole percent $PbZrO_3$ compositions (see Figure 33). Small amounts of ZrO_2 (see page 46) may be present as the only other phase in this range, except for the sample of pure $PbZrO_3$. As the $BiFeO_3$ content is increased in this range, the splitting of some pairs of lines on the individual patterns, such as (120) and (002), (240) and (004), etc., decreases until a composition of 80 mole percent $PbZrO_3$ is reached. At the 80 mole percent $PbZrO_3$-$BiFeO_3$ composition, these pairs of lines superimpose into single peaks and some of the superlattice lines, e.g., (110) and (041), disappear, making patterns of this composition nearly cubic except for two or three very small peaks, barely visible above the background. Samples in the range from 80 to 30 mole percent $PbZrO_3$ show a more pronounced distortion than for the 80 mole percent $PbZrO_3$ but appear to belong to the same orthorhombic phase.

In the range from 80-30 mole percent $PbZrO_3$, one weak line with $d \simeq 3.16Å$ is present on all patterns and does not vary its d value with composition. It doubtless corresponds to the major peak of ZrO_2. This peak with $d \simeq 3.16Å$ appears at the same d value as found on the patterns of the samples in the range from 95-81.81 mole percent $PbZrO_3$ (see also page 46). The other two peaks can be indexed in the orthorhombic system. Using the best resolving power of the Siemens Diffractometer, a 0.1° slit and a rate scan of 0.1°/min, the peak between 44° and 45° (2 θ) on the patterns of the 60 mole percent $PbZrO_3$ sample, which formerly was resolved clearly as two lines (200, 002) (tetragonal indexing) on the patterns of the 81.81 mole percent $PbZrO_3$ can not be resolved into more than one peak. This precludes tetragonal indexing for samples in the range of 80-30 mole percent $PbZrO_3$. Dielectrical measurements* of samples of pure $PbZrO_3$ to 81.81 mole percent $PbZrO_3$ suggest antiferroelectric behavior, and from 80-50 mole percent $PbZrO_3$ ferroelectric behavior. Samples with a composition higher than 50 mole percent $BiFeO_3$ are too conductive for meaningful dielectric measurements. At a composition of 80 mole percent $PbZrO_3$, a minimum in the Curie point is found, Figure 34. This may be explained on the basis that the structure is nearly cubic resulting in minimum distortion and accordingly a lower Curie point. However, the electrical properties and the non-cubic x-ray peaks for samples in the range from 80-50 mole percent $PbZrO_3$ suggest these materials are not cubic. Calculations show that samples in this range can be indexed on an orthorhombic multiple cell basis with the relations between

---

* Electrical measurements were performed in the Department of Physics by co-workers

the parameters only slightly different from the samples in the range of 100-81.81 mole percent $PbZrO_3$. In the composition range from 100-81.81 mole percent $PbZrO_3$, the tetragonal parameter a_o is only slightly different from c_o (c_o/a_o = 0.9904) and $c \cong 2c_o$ for each composition in the range, but in the range from 80-50 mole percent $PbZrO_3$, a_o is equal to c_o and $c \cong 2c_o = 2a_o$ (see also Table VI). The x-ray patterns of the samples in the range of 50-30 mole percent $PbZrO_3$ are essentially the same as that of 80-50 mole percent $PbZrO_3$. This structural arrangement explains the ferroelectric properties and the superlattice lines of the samples in this range.

As $BiFeO_3$ is added to $PbZrO_3$, distortion of the $PbZrO_3$ structure is reduced gradually. This can be seen from the tendency of some of the double peaks to coalesce by the decrease in the Curie point, Figure 34, in the range from 100-81.81 mole percent $PbZrO_3$. From 80-30 mole percent $PbZrO_3$, the Pb and Zr atoms together with Bi and Fe are occupying positions not too far removed from their original positions in the cubic perovskite lattice and the ZrO_6 octahedra is possibly less distorted. This may explain why the x-ray patterns of samples in the range are close to cubic. Furthermore the energy of the switching field required to reverse the polarization along the [001] direction would be reduced considerably, due to the decreased shift of the Pb and Bi atoms of the sublattices in the (001) plane. Additionally as the distortion of the oxygen octahedra is diminished, a reversal of polarization is further enhanced. The hysteresis loop obtained on a sample of 70 mole percent $PbZrO_3$ by the Physics group confirms this model. However, oxygen contributions to x-ray scattering are so small as compared to that of the heavy atoms, that there is no hope of confirming the oxygen shifts by conventional x-ray methods. Therefore, neutron diffraction analysis will be necessary to determine the extent of shift of all atoms from a cubic arrangement. Optical studies of single crystals would also prove helpful inasmuch as the model proposed, herein, would require a large optical anisotropy within the ab plane if the orthorhombic phase persists over such a large compositional range. Piezoelectric measurements would also provide a means of determining whether or not a non-centrosymmetric space group is also required over the range mentioned.

X-ray patterns of air-quenched samples suggest a transition in the region of approximately 30-25 mole percent $PbZrO_3$ to rhombohedral, though the splitting of the peak at 31.62° (2θ) on patterns of the 30 mole percent samples into two lines can not be seen until the composition of 15 mole percent $PbZrO_3$ in the rhombohedral phase is reached as examined by the Norelco Diffractometer. The Siemens Diffractometer, with a much higher resolving power, may be more helpful for an observation of this splitting. It is interesting to note that the transition for non-quenched samples occurs in the range 35-30 mole percent $PbZrO_3$, indicating the importance of a knowledge of the thermal history of the samples when stating phase widths and transitions. From 30 to 0 mole percent $PbZrO_3$, the structure is rhombohedral with parameters α and a changing only slightly, Figure 33. Excess γ-Bi_2O_3 is present in the sintered samples. The $Bi_2O_3 \cdot 2Fe_2O_3$ phase appears when the $BiFeO_3$ composition reaches 95 mole percent and it increases in amount for 100 percent $BiFeO_3$ samples prepared from equimolar mixtures of Bi_2O_3 and Fe_2O_3. Rhombohedral x-ray patterns of $BiFeO_3$ and orthorhombic patterns of $Bi_2O_3 \cdot 2Fe_2O_3$ are in good accord with the reports of Filip'ev[22] and Hideo Koizumi[27] (see Appendices B and C). Resolution for the two strongest rhombohedral lines on patterns of the samples in the range from 85-100 mole percent $BiFeO_3$ was achieved by using the Norelco Diffractometer at a scanning rate of 0.125°/min. A two-phase region is suggested in the region 30-25 mole percent $PbZrO_3$, similar to that reported for the $PbTiO_3$-$BiFeO_3$[29] system. Further study is required in this compositional range.

In preparing x-ray pure $BiFeO_3$ samples, increasing the Bi_2O_3 to Fe_2O_3 mole ratio from equimolar to 1.10:1.00 greatly decreased the proportion of the $Bi_2O_3 \cdot 2Fe_2O_3$ phase. As the mole ratio of Bi_2O_3 to Fe_2O_3 reached 1.50 to 1.00 and 2.00 to 1.00, the $Bi_2O_3 \cdot 2Fe_2O_3$ phase completely disappeared and the excess γ-Bi_2O_3 in the sintered samples was removed by warm concentrated nitric acid, since the solution rate of $BiFeO_3$ in this acid is considerably lower than that of $Bi_2O_3 \cdot 2Fe_2O_3$.

Phases present in each composition of the $PbZrO_3$-$BiFeO_3$ system are listed in Table VI. Since impurities may affect dielectric measurements considerable, pure samples of the system are, therefore, necessary. As discussed in the last section, evaporation of PbO from samples containing $BiFeO_3$ may lead to incomplete reactions. Closing the tube containing the samples during sintering had no obvious effect in reducing PbO losses. Therefore, excess PbO was added to several of the mixed oxides. When 5 mole percent excess PbO was added to the mixed oxides in preparing a 60 mole percent $PbZrO_3$ sample, ZrO_2 lines on the x-ray patterns of the sample decreased. However, the weight loss of PbO in the mixed oxides during sintering was found to be only one fifth of the excess PbO originally added, and neither the excess PbO left in the sample nor any new phase was found on the x-ray patterns. Amounts of 5-50 mole percent excess PbO were added in preparing 50 mole percent $PbZrO_3$ samples but the intensity of the ZrO_2 lines in the x-ray patterns was still found to be quite considerably. Therefore, preparation of pure samples employing mixtures of pure $PbZrO_3$

and pure $BiFeO_3$ powders rather than the four oxides might be quite useful.

High temperature x-ray analysis will be necessary to establish a phase diagram for the system. This analysis would be useful for investigating the dielectric properties of the system and for determination of the Curie point of $BiFeO_3$.

A plot of volume of one unit cell versus composition of this system is shown in Figure 35. Abrupt changes of the slopes of the curves in this figure, as seen from the points on the curves at the 81.81 and 80 mole percent $PbZrO_3$ as well as the 30 and 25 mole percent compositions, also give more evidence for the phase changes of the $PbZrO_3$-$BiFeO_3$ system. For the samples in the range of 100-81.81 mole percent of $PbZrO_3$ of the system, a suggested orthorhombic multiple cell structure with a = 2b is deduced reasonably from the proposed model confirmed by Jana et al.[17] for $PbZrO_3$ (see page 24 and Figure 12). From x-ray analysis, the a = 2b relation of the multiple cell is also employed in the structure determination for the samples in the 80-30 mole percent $PbZrO_3$ range. The equality, a = 2b, in this compositional range may be explained on the basis that the metal atoms, Pb, and Bi, as well as the oxygen octahedra may all shift back approximately to the positions of an ideal cubic perovskite lattice. However, a detailed study of the shift of all the atoms will require neutron diffraction analysis of the system.

C. MICROSCOPIC ANALYSIS

The photomicrographs of the $PbZrO_3$-$BiFeO_3$ system, are shown in Figures 36-49. The dark microporosity accounts for the failure to obtain theoretical densities for the hot-pressed samples, listed in Table VII. Some gray grains can be seen clearly in most of the photomicrographs, especially those of the unetched samples. These gray gains may be caused by microporosity just below the surface of the polished samples. Photomicrographs of unetched samples are used for comparison with those of the same samples after etching.

In Figure 37, the small grain size of the 80 mole percent $PbZrO_3$ sample is clearly visible and it appears to be homogeneous in line with the x-ray patterns. For the 63 mole percent $PbZrO_3$ sample, as seen in Figure 39, the small grains are almost the same size as shown in Figure 37, but the sample appears to be non-homogeneous. This is probably due to the presence of ZrO_2 as evidenced by x-ray analysis. In the photomicrograph of a 50 mole percent $PbZrO_3$ sample, Figure 41, the boundaries between two different kinds of grains, one white and one gray, are very clear. This lends some support to the results of x-ray analysis of the sample that there are at least two phases present. In Figure 43, a 25 mole percent $PbZrO_3$ sample exhibits two different types of grains, one gray in color, of generally small size, and one white

TABLE VI

X-ray data on the $PbZrO_3$-$BiFeO_3$ system

Sample No.	Mole % $PbZrO_3$	Parameters a (Å)	b (Å)	c (Å)	α (°)	Vol. of One Unit Cell† (Å^3)	Phases Present
A-3	100	5.873	11.746	8.228		70.950	Orthorhombic I.
C-2	95	5.869	11.738	8.223		70.810	Orthorhombic I with one or possibly two weak lines of ZrO_2.
C-4	90.47	5.864	11.728	8.216		70.629	Same as 95% composition.
C-5	85	5.850	11.700	8.212		70.258	Orthorhombic I with two weak lines of ZrO_2.
C-7	81.81	5.842	11.684	8.214		70.083	Same as 85% composition.
C-8	80	5.830	11.660	8.246		70.068	Orthorhombic II* or pseudocubic perovskite with one weak line of ZrO_2.

† The volume of this unit cell of the orthorhombic phases is one eighth the volume of the multiple cell as calculated from the product of the parameters a, b and c.

* The relationship between the parameters of the orthorhombic II phase is slightly different from that of the orthorhombic I phase (see page 51).

TABLE VI (Cont'd)

Sample No.	Mole % $PbZrO_3$	Parameters a (Å)	b (Å)	c (Å)	α (°)	Vol. of One Unit Cell† (Å^3)	Phases Present
C-10	75	5.820	11.640	8.230		69.692	Same as 80% composition except with one additional weak line of ZrO_2.
C-12	70	5.808	11.616	8.214		69.270	Same as 75% composition.
C-16	60	5.781	11.562	8.175		68.302	Same as 75% composition.
C-18	50	5.751	11.502	8.133		67.248	Same as 75% composition, with stronger ZrO_2 lines and possibly small amounts of other phases.@
C-23	35	5.679	11.358	8.029		64.736	Same as 50% composition.
C-25	30	5.655	11.310	7.990		63.876	Same as 50% composition except that the line corresponding to the main ZrO_2 line is shifted about 0.18 degree (2θ).

† See page 57.

@ These other phases are not identified clearly yet.

TABLE VI (Cont'd)

Sample No.	Mole % $PbZrO_3$	Parameters a (Å)	b (Å)	c (Å)	α (°)	Vol. of One Unit Cell† (Å^3)	Phases Present
C-27	25	3.985			**		Rhebohedral with γ-Bi_2O_3 and ZrO_2 lines.
C-29	20	3.981			89.290	63.037	Same as 25% composition with stronger γ-Bi_2O_3 and weaker ZrO_2 lines.
C-31	15	3.976			89.283	62.847	Same as 20% composition with stronger γ-Bi_2O_3 and weaker ZrO_2 lines.
C-33	11.11	3.974			89.276	62.767	Same as 15% composition.
C-35	5	3.965			89.266	62.326	Same as 15% composition except ZrO_2 disappeared and weak $Bi_2O_3 \cdot 2Fe_2O_3$ phase can be seen.
B-6	0	3.951			89.265	61.668	Same as 5% composition with stronger γ-Bi_2O_3 and $Bi_2O_3 \cdot 2Fe_2O_3$ lines.

† See page 57.

** Because there is no clearly divided pair of lines such as d_{hkl} and $d_{hk\bar{l}}$ on the x-ray patterns of the samples of this composition, the value of α_{rhomb} can not be calculated.

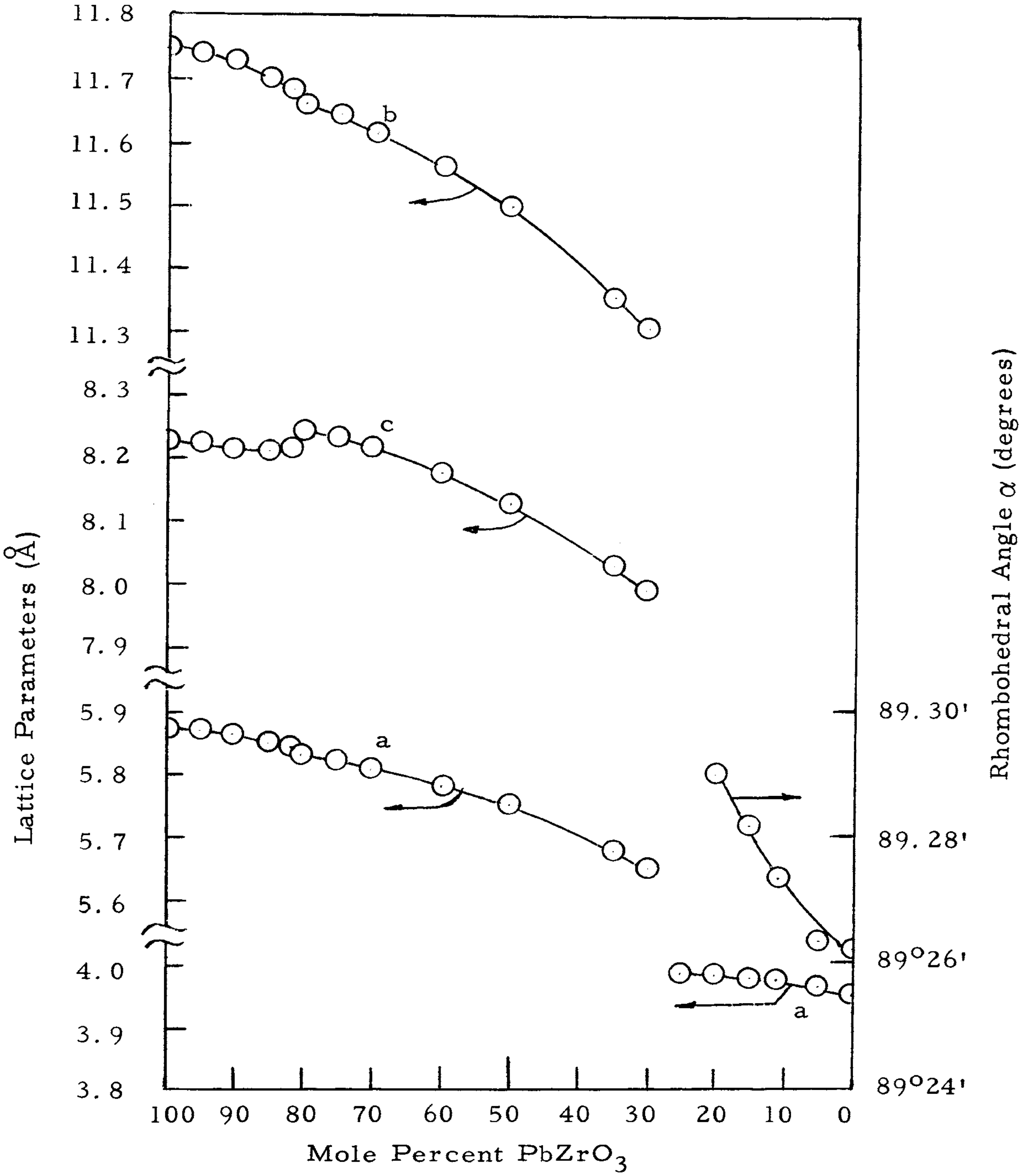

Figure 33. Lattice parameters of the $PbZrO_3$-$BiFeO_3$ System.

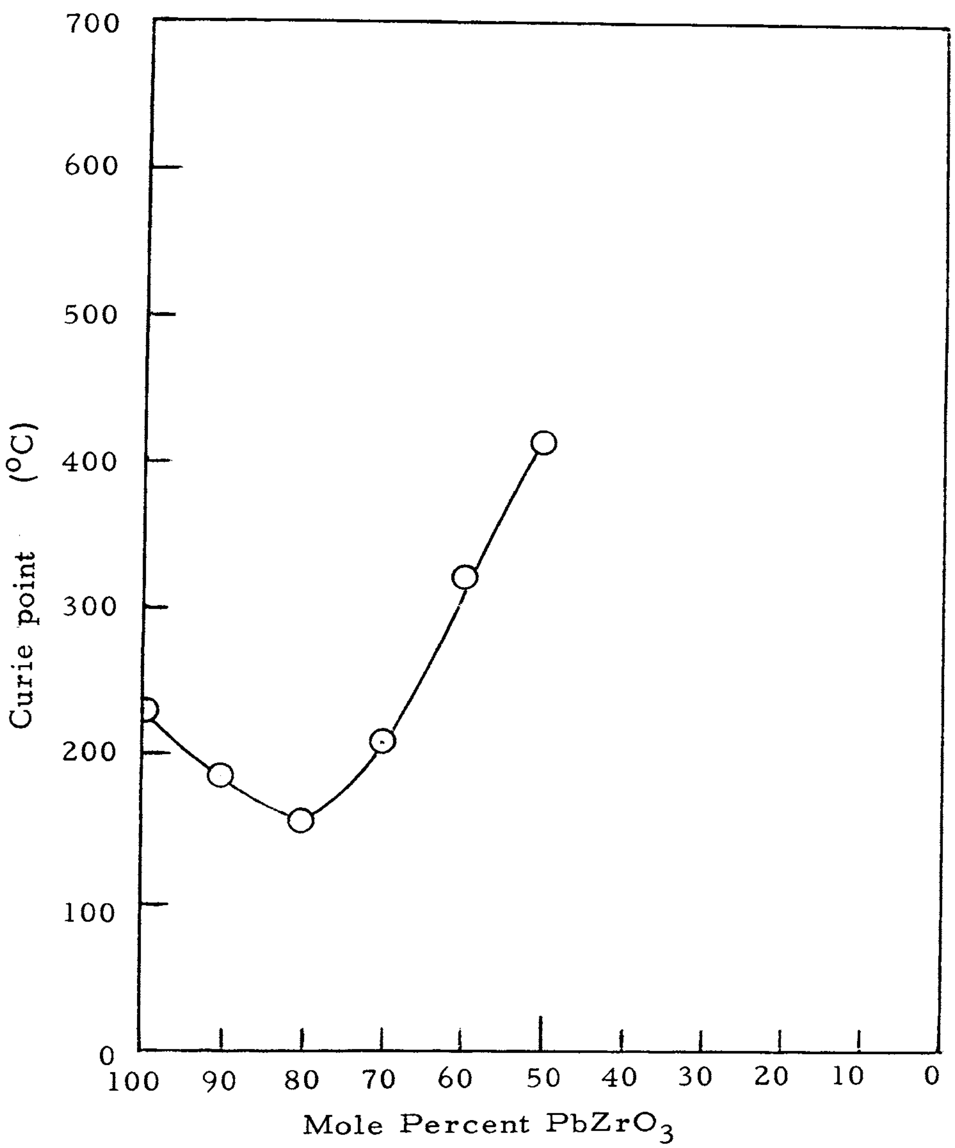

Figure 34. Curie point* versus composition of the $PbZrO_3$-$BiFeO_3$ system

* See page 50.

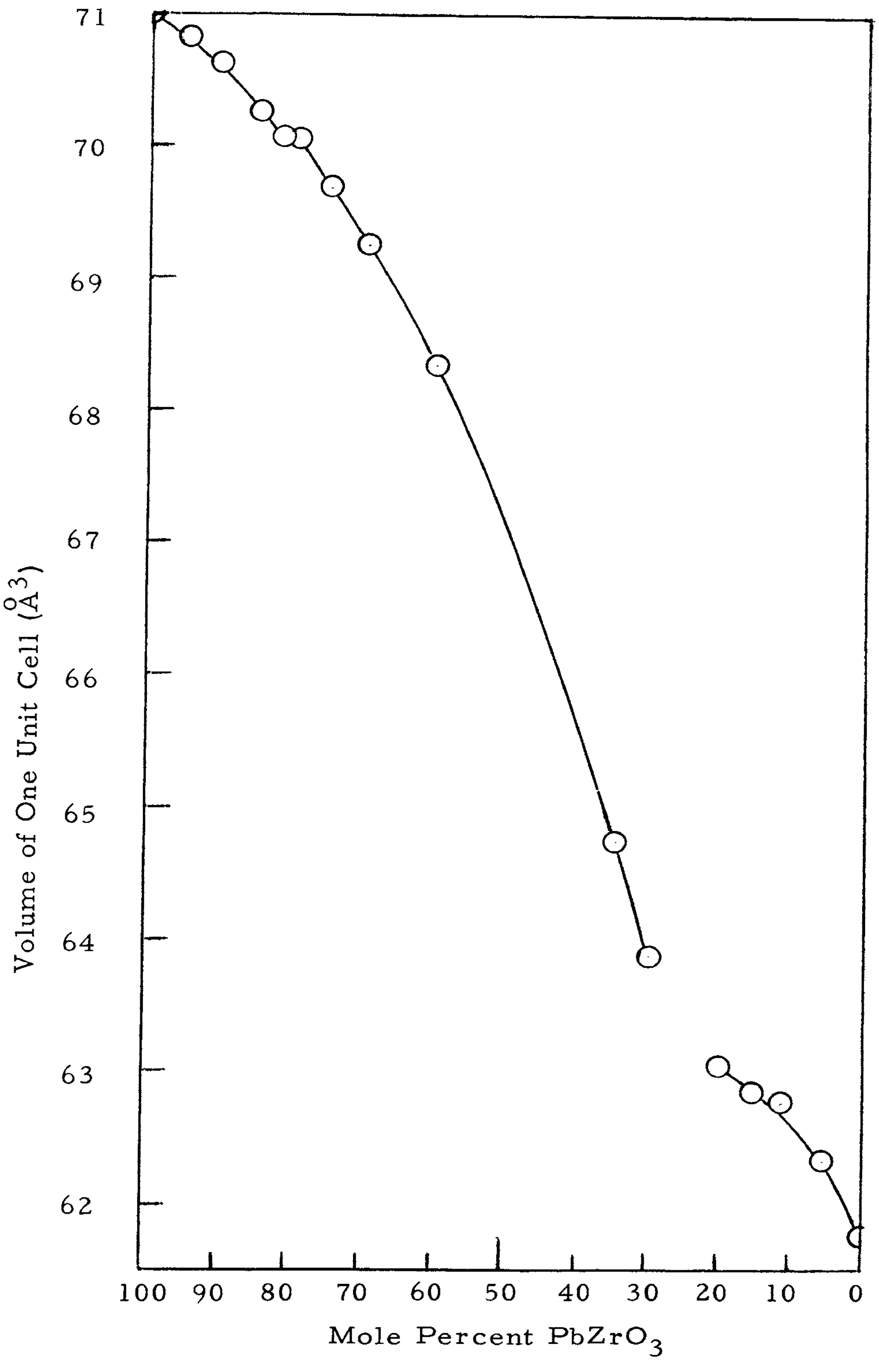

Figure 35. Variation of the volume of the unit cell for the $PbZrO_3$-$BiFeO_3$ system.

in color of larger size. They are poorly defined but are still observable. Perhaps a longer etching time is necessary for this composition. X-ray patterns of the 25 mole percent $PbZrO_3$ samples also show quite large amounts of a second phase, γ-Bi_2O_3. It was difficult to analyze the photomicrographs of the $BiFeO_3$ samples sintered from equimolar mixtures of Bi_2O_3 and Fe_2O_3. However, from the obviously non-homogeneous appearance of the pictures of these $BiFeO_3$ samples, it is impossible to interprete the samples as single phase. The x-ray evidence conclusively shows them to be multiphase.

Observations for the determination of both the number of phases and of ferroelectric domains for the samples of the $PbZrO_3$-$BiFeO_3$ system is important. Therefore, electron microscopic and electron microprobe analysis of powders and crystals would be of great value for further study.

TABLE VII

Samples of the $PbZrO_3$-$BiFeO_3$ system, hot pressed for microscopic study. *

Sample No.	Sample No. before Hot Pressing	Composition (Mole % $PbZrO_3$)	Time (hrs.)	Temperature (^oC)	Pressure** (psi)	Density@ (g/cm^3)
C-8-1	C-8	80	1	870	15000	
C-14-1	C-14	63	1	793	10000	
C-18-1	C-18	50	1	745	10000	
C-27-1	C-27	25	1	750	25000	
C-27-2	C-27	25	1	740	15000	8.00
B-4-1	B-4	0	0.58	720	15000	7.64
B-4-2	B-4	0	0.50	740	17000	8.15
D-1†		0	1	750	15000	
B-11-1	B-11	$Bi_2O_3 \cdot 2Fe_2O_3$	1	745	10000	

* See page 40.

** During hot pressing, each sample was surrounded by MgO powder; therefore the pressure listed is not very accurate.

@ See page 40.

† This sample was originally made by Mr. Gary D. Achenbach who removed the γ-Bi_2O_3 from the sample by using concentrated hydrochloric acid and nitric acid.

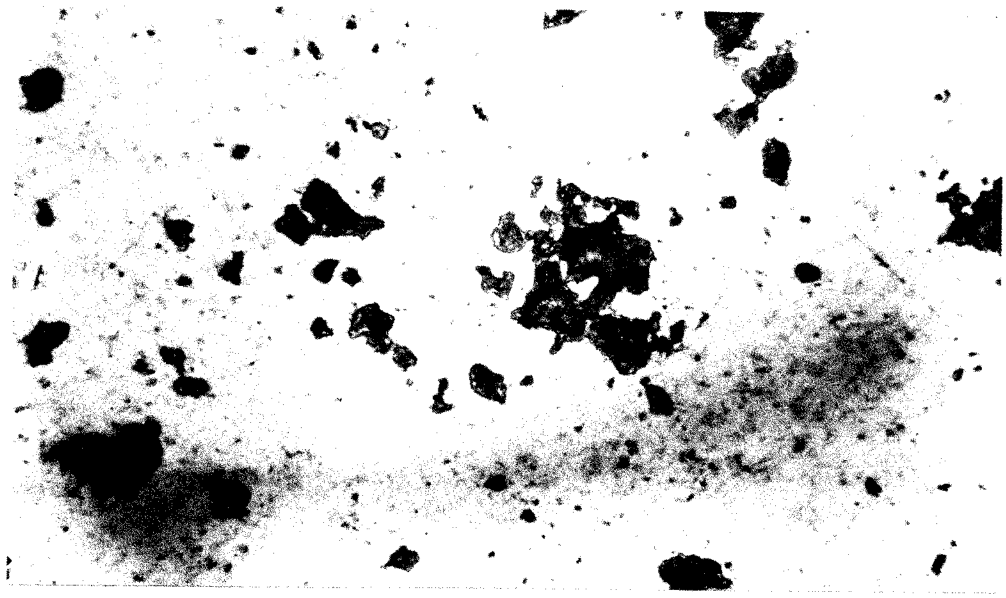

Figure 36. Photomicrograph of 80% $PbZrO_3$-20% $BiFeO_3$ Sample C-8-1, not etched, viewed in reflected light. 500x.

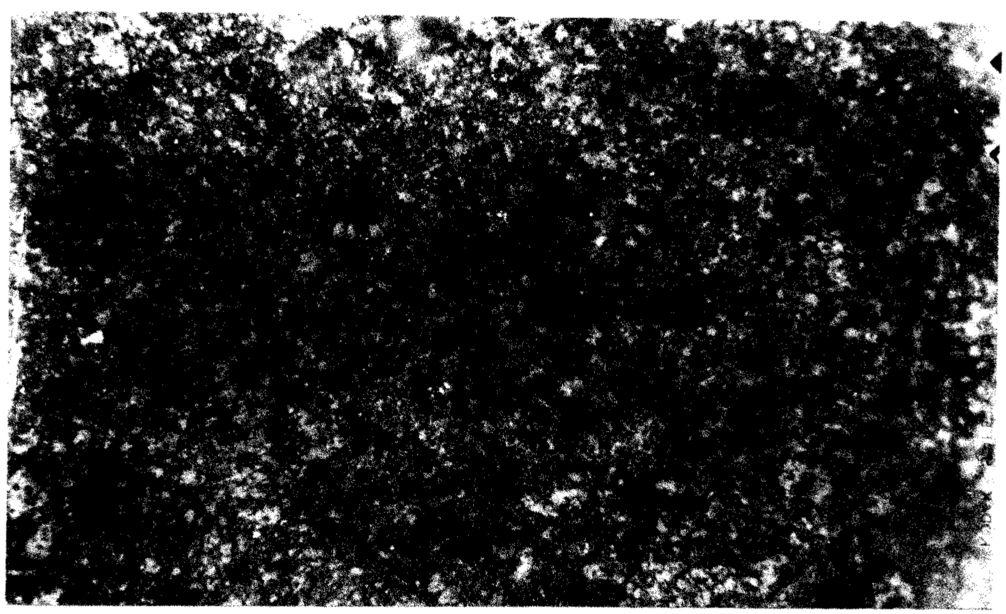

Figure 37. Photomicrograph of 80% $PbZrO_3$-20% $BiFeO_3$ Sample C-8-1, etched 1/3 second, viewed in reflected light using a blue filter. 1000x.

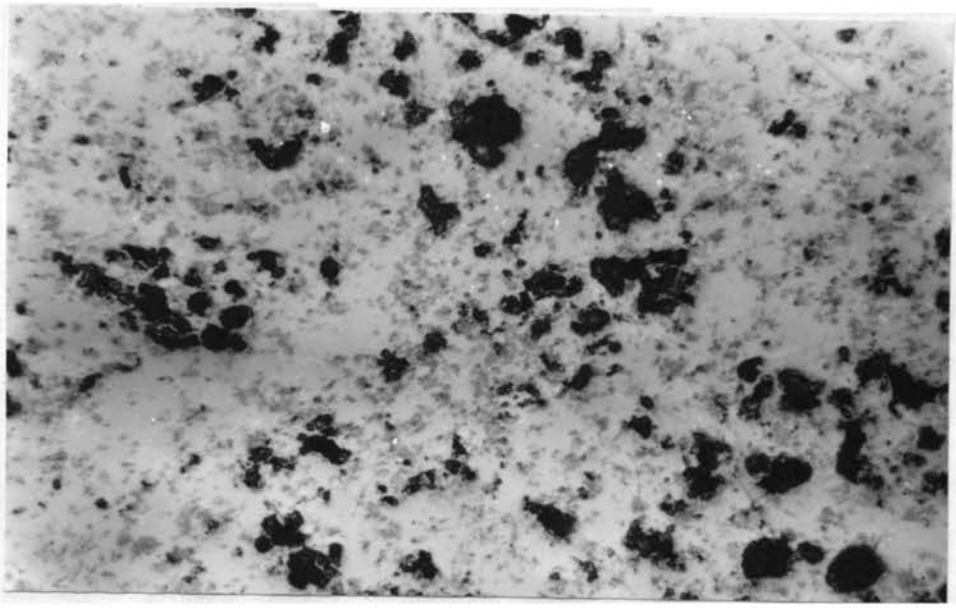

Figure 38. Photomicrograph of 63% $PbZrO_3$-37% $BiFeO_3$ sample C-14-1, not etched, viewed in reflected light. 500x.

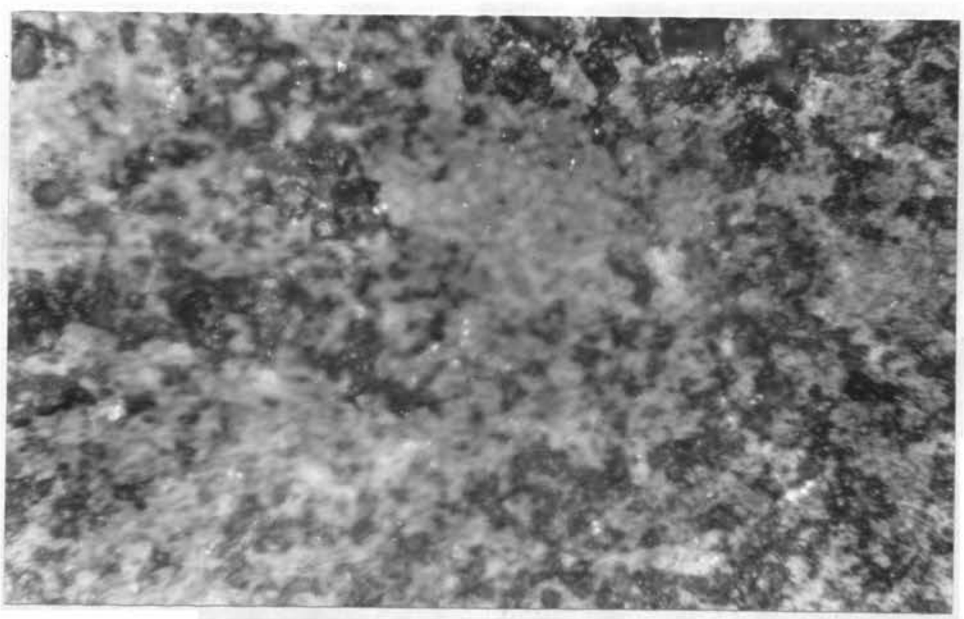

Figure 39. Photomicrograph of 63% $PbZrO_3$-37% $BiFeO_3$ sample C-14-1, etched 1 second, viewed in reflected light. 1000x.

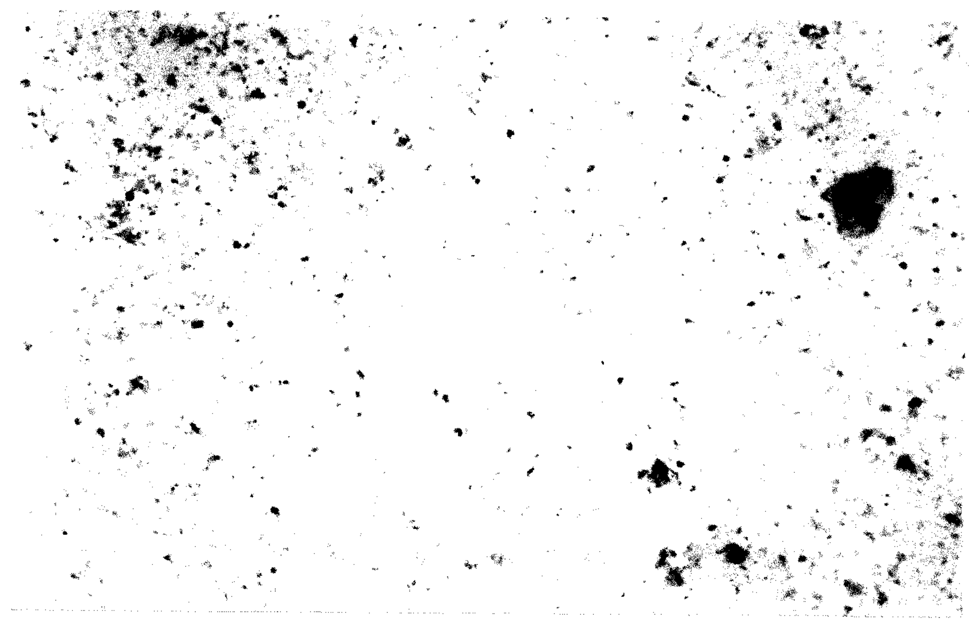

Figure 40. Photomicrograph of 50% $PbZrO_3$-50% $BiFeO_3$ sample C-18-1, not etched, viewed in reflected light. 500x.

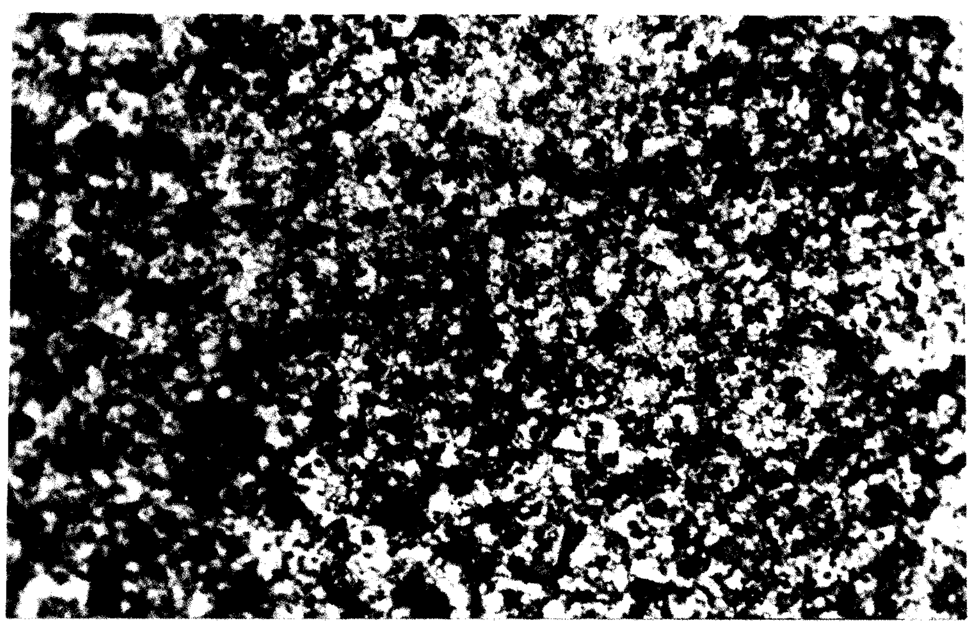

Figure 41. Photomicrograph of 50% $PbZrO_3$-50% $BiFeO_3$ sample C-18-1, etched 2 seconds, viewed in reflected light. 1000x.

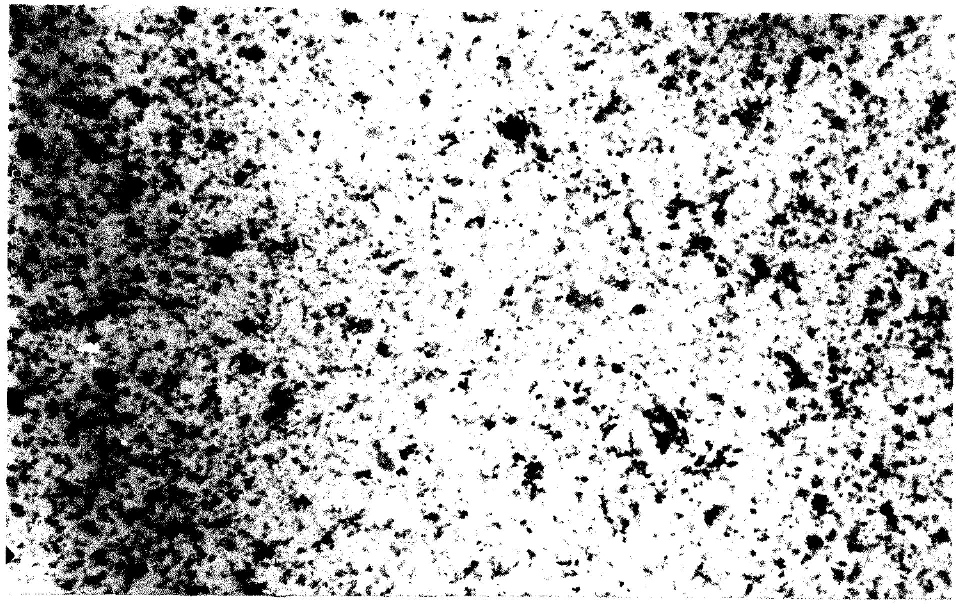

Figure 42 Photomicrograph of 25% $PbZrO_3$-25% $BiFeO_3$ sample C-27-1, not etched, viewed in reflected light. 500x.

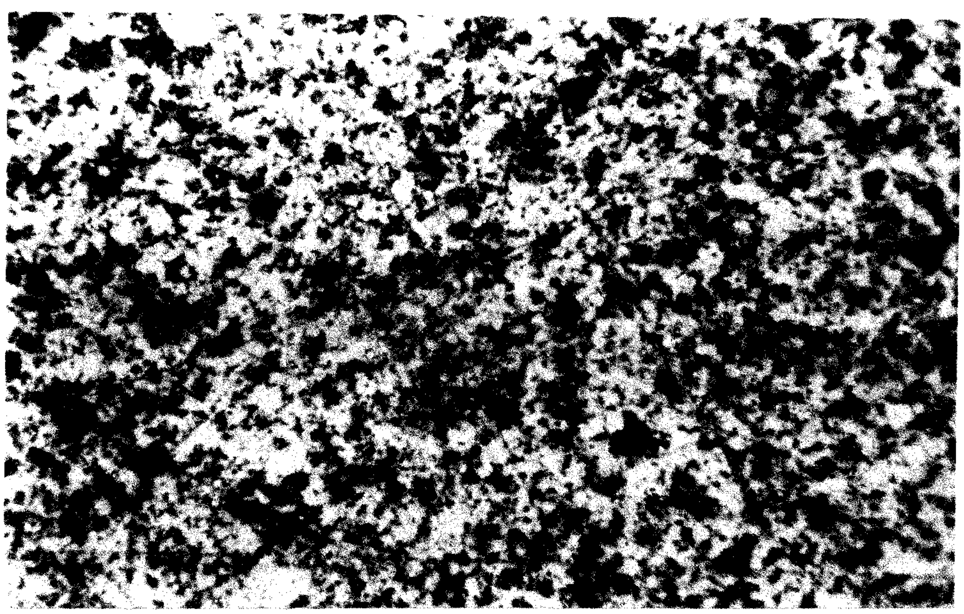

Figure 43. Photomicrograph of 25% $PbZrO_3$-25% $BiFeO_3$ sample C-27-1, etched 5 seconds, viewed in reflected light. 1000x.

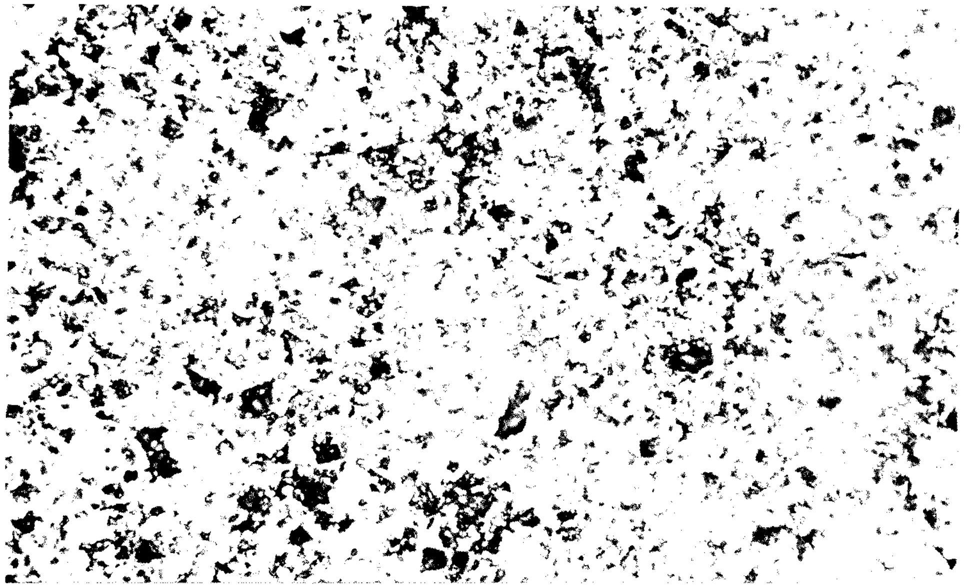

Figure 44. Photomicrograph of 100% $BiFeO_3$ sample B-4-1, not etched, viewed in reflected light. 500x.

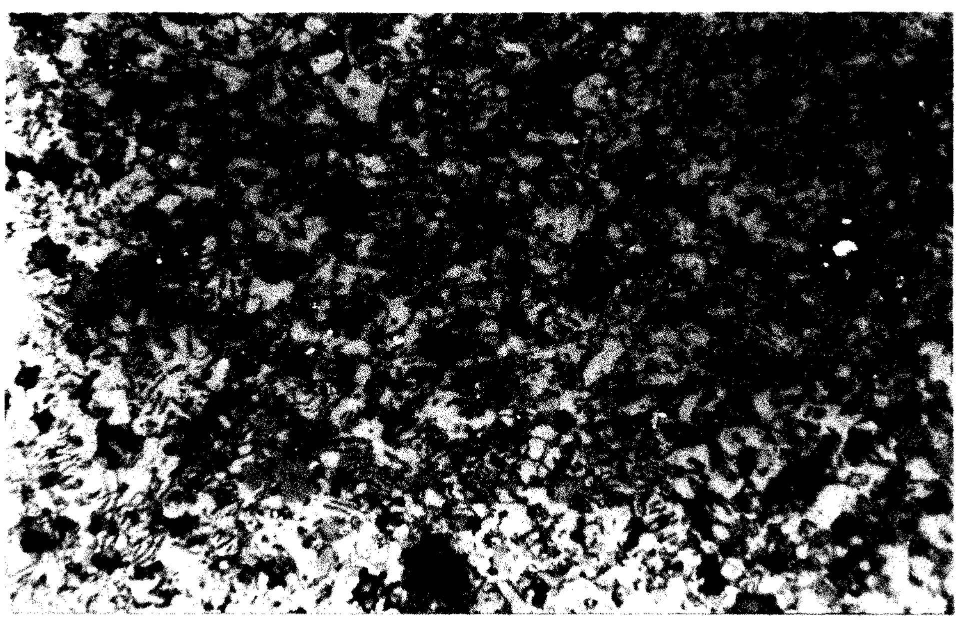

Figure 45. Photomicrograph of 100% $BiFeO_3$ sample B-4-1, etched 4 seconds, viewed in reflected light. 1000x.

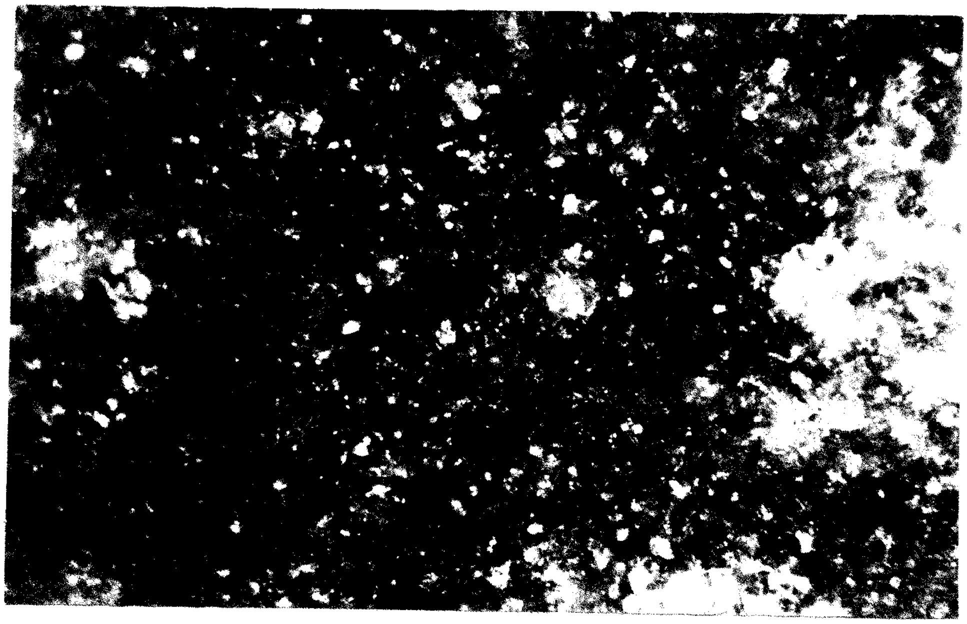

Figure 46. Photomicrograph of 100% $BiFeO_3$ sample B-4-1, etched 4 seconds, viewed in polarized light. 1000x.

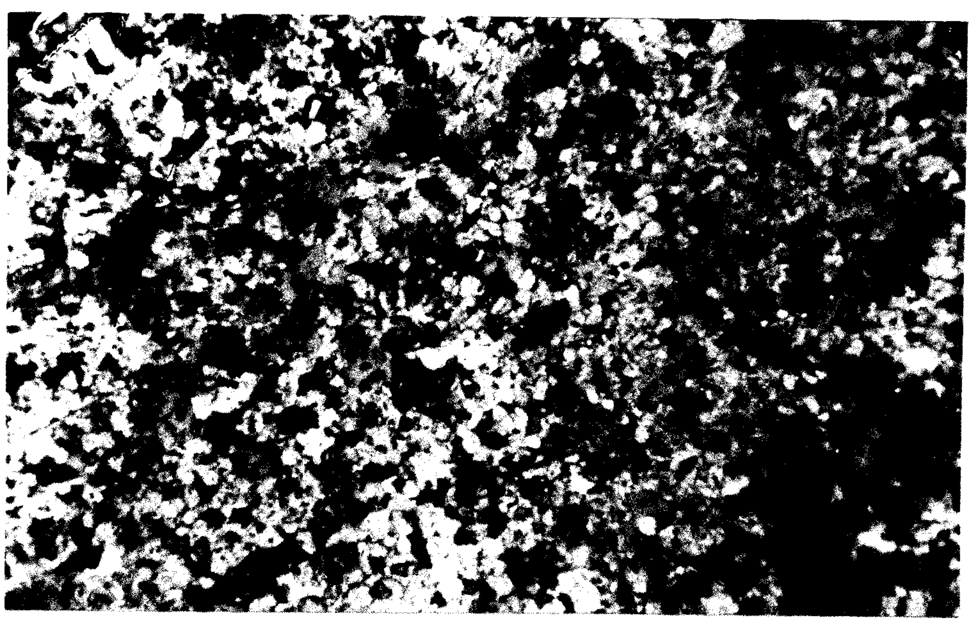

Figure 47. Photomicrograph of 100% $BiFeO_3$ sample B-4-1, etched 30 seconds in 1% HCl and 1% HNO_3 (by weight), viewed in reflected light. 1000x.

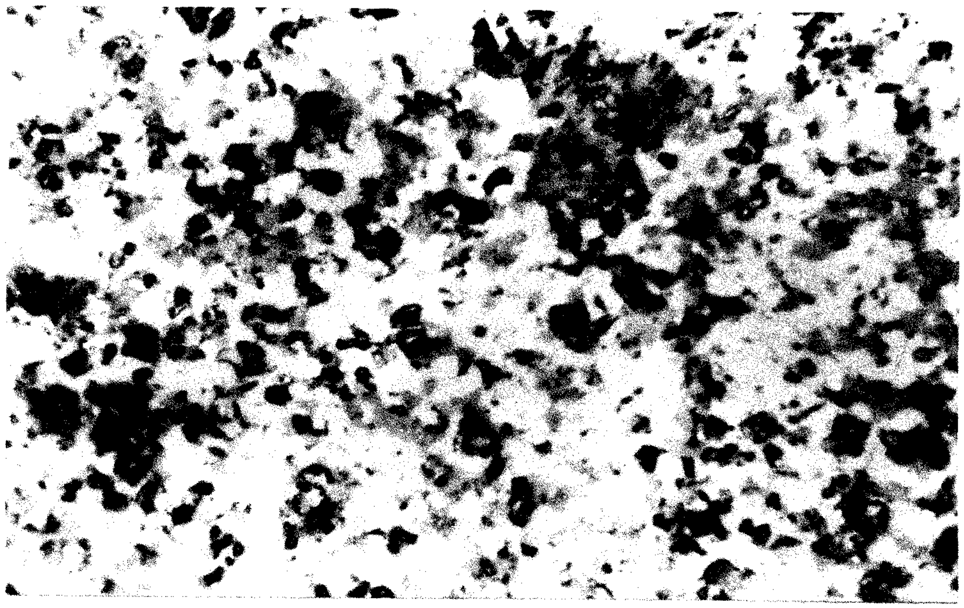

Figure 48. Photomicrograph of 100% $BiFeO_3$ sample D-1, not etched, viewed in reflected light. 1000x.

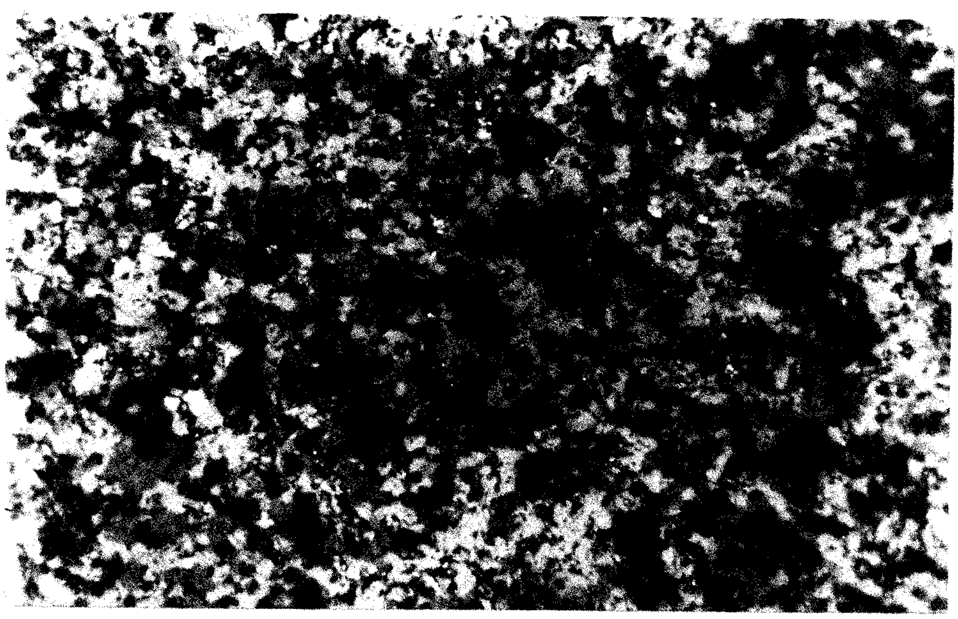

Figure 49. Photomicrograph of 100% $BiFeO_3$ sample D-1, etched 4 seconds, viewed in reflected light. 1000x.

V. SUMMARY AND CONCLUSIONS

For the system of lead zirconate-bismuth ferrate several conclusions were reached.

1. The samples prepared for this system appear to be solid solutions over the entire compositional range except for small amounts of impurity phases in some regions and possibly a small two-phase region in the area of the orthorhombic to rhombohedral transition. From 100 to approximately 30 mole percent $PbZrO_3$, an orthorhombic multiple cell structure (see Table VI) is proposed with a rhombohedral arrangement from 25 to 0 mole percent $PbZrO_3$, as determined by x-ray analysis and microscopic observation. A two phase region similar to the case reported for the $PbTiO_3$-$BiFeO_3$ system[29] may exist between the compositions of 30 and 25 mole percent $PbZrO_3$.

2. Antiferroelectric and ferroelectric properties are suggested from electrical measurements* over the regions 100-81.81 and 80-50 mole percent $PbZrO_3$ respectively. A minimum in the Curie point occurs at approximately 80 mole percent $PbZrO_3$, Figure 34. Consistent with these results is the presence of a nearly cubic structure at the same composition on the x-ray patterns. Samples

---

* see page 50.

with $BiFeO_3$ composition of more than 50 mole percent are too conductive for meaningful dielectric measurements.

The electrical properties of these compositions can be explained on the basis of the structural model proposed by Jona et al.[16] for pure $PbZrO_3$.

3. An additional orthorhombic phase of $Bi_2O_3 \cdot 2Fe_2O_3$ was found in the samples of $BiFeO_3$ prepared from equimolar mixtures of Bi_2O_3 and Fe_2O_3. X-ray pure $BiFeO_3$ samples can be made by using excess Bi_2O_3 (1.50 mole Bi_2O_3:1.00 mole Fe_2O_3), sintering, followed by subsequent leaching of the excess Bi_2O_3 in concentrated nitric acid.

4. As the use of x-ray analysis for light atoms is limited, neutron diffraction analysis will be necessary to determine the extent of shift of all atoms from a cubic arrangement. High temperature x-ray analysis would be useful in construction of a phase diagram for the system. Electron microscopic and microprobe studies would be helpful for determining the number of phases present in each sample of the system as well as ferroelectric domains in some of the samples of the system. For the samples with high $BiFeO_3$ composition, neutron diffraction studies should reveal any magnetic structure present. If single crystals of the system could be prepared, optical measurements would be useful for structural analysis of the crystals. All of the experimental methods described should provide an insight into the nature of the chemical bonding in these systems.

BIBLIOGRAPHY

1. SCHWALLER, J.J. (1963) A Preliminary Study of the Dielectric Properties of Bismuth Ferrate Ceramics. Thesis, University of Missouri at Rolla. 71 p. (with 28 figr., 9 tables.)

2. BERLINCOURT, D.A., KRUEGER, H.H.A. (1963). Annual Progress Report, 1963, Sandia Corporation; Purchase Order 51-6529, March 16, 1964.

3. MEGAW, H.D. (1957) Ferroelectricity in Crystals. Methuen and Co. Ltd., London. 220 p.

4. KITTEL, C. (1951) Antiferroelectric Crystals. Phys. Rev. 82, p. 729.

5. SHIRANE, G., SAWAGUCHI, E. and TAKAGI, Y. (1951) Dielectric Properties of Lead Zirconate. Structure Reports 15, pp. 195-196.

6. KANZIG, W. (1957) Ferroelectricics and Antiferroelectricics. Academic Press, New York and London. 197 p.

7. KITTEL, C. (1963) Introduction to Solid State Physics. 2nd ed., John Wiley & Sons, Inc., New York. 617 p.

8. ROTH, R.S. (1957) Classification of Perovskite and Other ABO_3-Type Compounds. J. Res. U.S. Natl. Bureau of Standards 58, 2, pp. 75-88.

9. PAULING, L. (1945) The Nature of the Chemical Bond. Cornell University Press, Ithaca. p. 514.

10. NARAY-SZABO, I. (1947) The Perovskite Family. Muegyetemi Kozlemenyek 1947, 1, pp. 30-41.

11. STILLWELL, C.W. (1938) Crystal Chemistry. 1st ed., McGraw-Hill Book Company, Inc., New York and London. pp. 265-275.

12. McQUARRIE, M. (1955) Barium Titanate and Other Ceramic Ferroelectrics:I. Introduction. Am. Ceram. Soc. Bull. 34, p. 171.

13. NARAY-SZABO, St. V. (1943) Die Struk-turtyp des Perowskites ($CaTiO_3$). Structure Reports 10, pp. 111-112.

14. MEGAW, H. D. (1946) Crystal Structure of Double Oxides of the Perovskite Type. Proc. Phys. Soc. 58, 2, pp. 133-152.

15. SAWAGUCHI, E., MANIWA, H. and HOSHINO, S. (1951) Antiferroelectric Structure of Lead Zirconate. Structure Reports 15, p. 195.

16. SAWAGUCHI, E. (1952) Lattice Constants of $PbZrO_3$. Structure Reports 16, pp. 254-255.

17. JONA, F., SHIRANE, G., MAZZI, F. and PEPINSKY, R. (1957) X-ray and Neutron Diffraction Study of Antiferroelectric Lead Zirconate, $PbZrO_3$. Phys. Rev. 105, 3, pp. 845-856.

18. ROBERTS, S. (1950) Dielectric Properties of Lead Zirconate and Barium-Lead Zirconate. J. Am. Ceram. Soc. 33, pp. 63-66.

19. McQUARRIE, M. (1955) Barium Titanate and Other Ceramic Ferroelectrics: III. Related Materials. Am. Ceram. Soc. Bull. 34, pp. 258-259.

20. SHIRANE, G., SUZUKI, K. and TAKEDA, A. (1952) Phase Transitions in Solid Solutions of $PbZrO_3$ and $PbTiO_3$. II. X-ray Study. Structure Reports 16, pp. 255-256.

21. SAWAGUCHI, E. (1953) Ferroelectricity versus Antiferroelectricity in the Solid solutions of $PbZrO_3$ and $PbTiO_3$. Structure Reports 17, pp. 433-435.

22. ROYEN, P. and SWARS, K. (1957) Das System Wismutoxyd-Eisenoxyd in Bereich von 0 bis 55 Mol % Eisenoxyd. Angew. Chem. 69, p. 779.

23. FILIP'EV, V.S., SMOLYANINOV, N.P. and FESENKO, E.G. (1960) Synthesis of $BiFeO_3$ and Determination of the Unit Cell. Soviet Physics-Cryst. 5, 6, pp. 913-914.

24. FEDULOV, S.A., VENEVTSEV, Y.N., ZHDANOV, G.S. and SMAZHEVSKAYA, E.G. (1961) High-Temperature X-ray and Thermal-Analysis Results for Bismuth Ferrite. Soviet Physics-Cryst. 6, 5, pp. 640-641.

25. ZASLAVSKII, A.I. and TUTOV, A.G. (1962) Structure of the New Antiferromagnetic $BiFeO_3$. Soviet Physics-Doklady 5, pp. 1257-1259.

26. FEDULOV, S.A., VENEVTSEV, Y.N., ZHELANOV, G.S., SMAZHEVSKAYA, E.G. and REJ, I.S. (1962) X-ray and Electrical Studies of the $PbTiO_3$-$BiFeO_3$ System. Soviet Physics-Cryst. 7, 1, pp. 62-66.

27. KOIZUM, H., NIZEKI, N. and IKEDA, T. (1964) An X-ray Study on Bi_2O_3-Fe_2O_3 System. Japan. J. App. Phys. 3, pp. 495-496.

28. KISELEV, S.V., OZENOV, R.P. and ZHDANOV, G.S. (1962) Detection of Magnetic Arrangement in $BiFeO_3$ Ferroelectric by Neutron Diffraction. Soviet Physics - Doklady 7, 8, pp. 742-744.

29. FEDULOV, S.A., LADYZHINSKII, P.B., PYATIGORSKAYA, I.L. and VENEVTSEV, Y.N. (1964) Complete Phase Diagram of the $PbTiO_3$-$BiFeO_3$ System. Soviet Physics-Solid State 6, 2, pp. 375-378.

30. ROGINSKAYA, Y.E., VENEVTSEV, Y.N., FEDULOV, S.A. and ZHDANOV, G.S. (1964) An X-ray Diffraction Investigation of the Magnetic and Electric Properties of the System $BiFeO_3$-$LaFeO_3$. Soviet Physics-Cryst. 8, 4, pp. 490-494.

31. KRAINIK, N.N., KHUCHUA, N.P., BEREZHNOI, A.A. and TUTOV, A.G. (1965) Nature of Phase Transformations in Solid Solutions of $BiFeO_3$ with $PbFe_{1/2}Nb_{1/2}O_3$. Soviet Physics-Solid State 7, 1, pp. 100-107.

32. ZHDANOVA, V.V. (1965)Dilatometric Study of Solid Solutions in the System $BiFeO_3$-$PbFe_{1/2}Nb_{1/2}O_3$. Soviet Physics-Solid State 7, 1, pp. 108-111.

33. BUHRER, C.F. (1962) Some Properties of Bismuth Perovskites. J. Chem. Phys. 36, 3, pp. 798-803.

34. TUTOV, A.G., MYL'NIKOVA, I.E., PARFENOVA, N.N., BOKOV, V.A. and KIZHAEV, S.A. (1964) New Compounds in the Systems Bi_2O_3-Me_2O_3 (Fe^{3+}, Al^{3+}, Ga^{3+}, Mn^{3+}). Soviet Physics-Solid State 6, 4, p. 963.

35. ROGINSKAYA, Y.E. and VENEVTSEV, Y.N. (1965) Investigation of the Structure and Magnetic Properties of Solid Solutions in the System $BiFeO_3$-$LaCrO_3$. Soviet Physics-Solid State 7, 2, pp. 321-325.

36. LANGE, N.A. (1956) Handbook of Chemistry. 9th ed., Handbook Publishers, Inc., Sandusky, Ohio. pp. 228-229.

37. ECONOMOS, G. (1959) Kinetics of High-Temperature Processes. W.D. Kingery, Editor. The Technology Press of Massachusetts Institute of Technology, John Wiley & Sons, Inc., New York, and Chapman & Hall, Limited, London, pp. 243-249.

APPENDIX A

Sintering Data

A. SINTERING DATA FOR THE $PbZrO_3$ SAMPLES

Sample No.	Composition of Mixed Oxides ($mP_bO+nZ_rO_2$)	Time (hrs)	Temp. (^oC)	Sintering System	Remarks*
A-1	1.00 + 1.00	2	870	Open	
A-2	1.00 + 1.00	2	870	Closed	
A-3	1.00 + 1.00	6	870	Closed	Air quenched
A-4	1.00 + 1.00	2	920	Open	
A-5	1.00 + 1.00	2	1200	Closed	
A-6	1.02 + 1.00	2	920	Closed	
A-7	1.02 + 1.00	2	1100	Closed	
A-8	1.06 + 1.00	2	1100	Closed	
A-9	1.15 + 1.00	{2	1200		
		{4	470	Open	
A-10	1.00 + 1.10	2	1200	Closed	

B. SINTERING DATA FOR THE $BiFeO_3$ SAMPLES

Sample No.	Composition of Mixed Oxides ($mBi_2O_3+nFe_2O_3$)	Time (hrs)	Temp. (^oC)	Sintering System	Remarks*
B-1	1.00 + 1.00	9	725	Closed	
B-2	1.00 + 1.00	3	750	Open	
B-3	1.00 + 1.00	6	750	Closed	Water quenched
B-4	1.00 + 1.00	2	800	Open	
B-5	1.00 + 1.00	2	810	Open	
B-6	1.00 + 1.00	2	850	Closed	
B-7	1.00 + 1.00	2.2	845	Closed	Air quenched
B-8	1.00 + 1.00	2.5	850	Closed	Mixed oxides pressed at 15000 psi

* The samples which are not noted as air or water quenched were left in the furnace to cool slowly to room temperature at the furnace cooling rate.

B. (Cont'd)

Sample No.	Composition of Mixed Oxides $mBi_2O_3+nFe_2O_3$	Time (hrs)	Temp. (°C)	Sintering System	Remarks*
B-9	1.00 + 1.12	2	800	Closed	
B-10†	1.00 + 2.00	2	800	Closed	
B-11	1.10 + 1.00	2	800	Open	
B-12	1.50 + 1.00	2	800	Closed	

C. SINTERING DATA FOR THE SAMPLES OF THE $PbZrO_3$-$BiFeO_3$ SYSTEM.

Sample No.	Composition** (mole% $PbZrO_3$)	Time (hrs)	Temp. (°C)	Sintering System	Remarks*
C-1	98.01	2	870	Open	
C-2	95	6	870	Closed	Air quenched
C-3	90.47	2	870	Open	
C-4	90.47	6	870	Closed	Air quenched
C-5	85	6	870	Closed	Air quenched
C-6	81.81	2	870	Open	
C-7	81.81	6	870	Closed	Air quenched
C-8	80	6	870	Closed	Air quenched
C-9	75	2	870	Open	
C-10	75	6	870	Closed	Air quenched
C-11	70	2	870	Closed	
C-12	70	6	870	Closed	Air quenched
C-13	66.66	2	870	Open	
C-14	63	2	870	Closed	
C-15	60	2	870	Closed	
C-16	60	6	870	Closed	Air quenched
C-17	50	2	870	Open	

---

* See page 78.

† The major phase present in this sintered sample is $Bi_2O_3 \cdot 2Fe_2O_3$.

** The samples of the $PbZrO_3$-$BiFeO_3$ system were prepared by sintering stoichiometric mixtures of corresponding oxides except those indicated specifically in the Remarks column.

C. (Cont'd)

Sample No.	Composition** (mole % $PbZrO_3$)	Time (hrs)	Temp. (^oC)	Sintering System	Remarks*
C-18	50	6	870	Closed	Air quenched
C-19	42.85	2	870	Open	
C-20	40	6.5	870	Closed	Air quenched
C-21	39.91	2	870	Open	Small amount of ZrO_2 added in excess
C-22	35	2	870	Closed	
C-23	35	6	870	Closed	Air quenched
C-24	30	2	870	Open	
C-25	30	6	870	Closed	Air quenched
C-26	25	2	870	Closed	
C-27	25	6	870	Closed	Air quenched
C-28	20	2	870	Closed	
C-29	20	6	870	Closed	Air quenched
C-30	15	2	870	Closed	
C-31	15	6	870	Closed	Air quenched
C-32	11.11	2	870	Closed	
C-33	11.11	6	870	Closed	Air quenched
C-34	5	2	870	Closed	
C-35	55	6	870	Closed	Air quenched
C-36	60	2	870	Closed	Air quenched and 5 mole % PbO added in excess.

** See page 79.

* See page 78.

APPENDIX B.

A. CALCULATED VALUES OF d and hkl FOR THE ORTHORHOMBIC MULTIPLE CELL OF $PbZrO_3$

With parameters, $a = 4.152 \times \sqrt{2} = 5.872$ (Å), $b = 4.152 \times 2\sqrt{2} = 11.744$ (Å) and $c = 4.101 \times 2 = 8.202$ (Å), reported by Etsuro Sawaguchi(16) at 20°C for CuKα radiation.

d	hkl
5.2521	110
4.1521	120
4.1010	002
3.2572	130
3.2323	112
3.0272	131
2.9360	200, 040
2.8483	210
2.7642	041, 201
2.5506	132
2.3873	042, 202
2.3488	050, 230
2.0761	240
2.0505	004
1.9307	310
1.8569	320
1.8385	124
1.7507	330
1.6916	322
1.6811	204, 044
1.6641	214
1.6101	332
1.5037	350
1.4680	400
1.4651	135
1.4589	244
1.4118	352
1.3726	412
1.3314	026
1.3130	440
1.3033	432
1.2449	450

A. (Cont'd)

d	hkl
1.1970	335
1.1815	236
1.1417	434
1.1249	530
1.1144	531
1.1087	522
1.1057	444
1.1009	326

B. X-RAY DATA FOR RHOMBOHEDRAL DISTORTED PEROVSKITE LATTICE OF $BiFeO_3$

Reported by:

Zaslavskii[25] for CuKα Radiation.
Filip'ev[23] for FeKα Radiation.

CuK Radiation			FeK Radiation		
hkl	Intensity	d value	hkl	Intensity	d value
100	140	3.946	100	4	3.96
110	171	2.809	110	10	2.82
$10\bar{3}$	161	2.782	$1\bar{1}0$	10	2.79
111	23	2.308	111	1	2.31
101	65	2.273	$\bar{1}11$		
200	100	1.976	$1\bar{1}1$	3	2.28
210	72	1.775	$11\bar{1}$		
201	37	1.761	200	4	1.98
211	45	1.626	210	5	1.78
$21\bar{1}$	83	1.613	$2\bar{1}0$	5	1.76
$11\bar{2}$	42	1.607	211	3	1.62
220	24	1.405	$\bar{2}11$		
$20\bar{2}$	23	1.390	$2\bar{1}1$	8	1.61
221	7	1.330	$21\bar{1}$		
300	6	1.319	220	2	1.406
$21\bar{2}$	36	1.314	$2\bar{2}0$	2	1.392
310	29	1.254	221	4	1.329

B. (Cont'd)

CuK Radiation

hkl	Intensity	d value
$30\bar{1}$	28	1.248
311	9	1.200
$31\bar{1}$	18	1.191
222	14	1.138
320	13	1.102
302	13	1.092
321	22	1.066
$32\bar{1}$	22	1.058
$31\bar{2}$	22	1.053

FeK Radiation

hkl	Intensity	d value
$22\bar{1}$, 300	4	1.317
$2\bar{2}1$, $\bar{2}21$	4	1.312
310	4	1.253
$3\bar{1}0$	4	1.245
311	1	1.214
$3\bar{1}1$, $31\bar{1}$	2	1.200
311	2	1.192
222	1	1.155
$\bar{2}22$, $2\bar{2}2$, $22\bar{2}$	3	1.138
220	5	1.103
$3\bar{2}0$	4	1.092
321	4	1.066
$32\bar{1}$	4	1.060
$3\bar{2}1$, $\bar{3}21$	7	1.053
400	2	0.989

C. X-RAY POWDER DIFFRACTION DATA OF $Bi_2O_3 \cdot 2Fe_2O_3$

Reported by:

Hideo Koizumi, Nobukazu Niizeki and Takuro Ikeda[27] for $CuK\alpha$ Radiation.

$d_{obs.}$ (Å)	$I_{obs.}$	$d_{cal.}$ (Å)	hkl
6.005	53	6.005	001
4.215	15	4.214	020
3.975	11	3.975	200
3.725	23	3.724	120
3.595	14	3.595	210
3.445	22	3.451	021

C. (Cont'd)

$d_{obs.}$ (Å)	$I_{obs.}$	$d_{cal.}$ (Å)	hkl
3.312	30	3.315	201
3.160	100	3.166	121
3.085	89	3.085	211
2.995	35	3.003	002
2.890	31	2.892	220
2.650	32	2.650	130
2.608	5	2.606	221
2.531	16	2.527	310
2.443	18	2.446	022
2.425	6	2.425	131
2.395	27	2.396	202
2.335	12	{2.338	122
		2.329}	311
2.304	27	2.305	212
2.246	3	2.243	320
2.141	22	2.144	231
2.039	17	2.037	140
1.997	6	2.002	003
1.987	8	{1.989	041
		1.987	400
		1.987}	132

Note: $d_{cal.}$ values are computed with the orthorhombic lattice constants; a = 7.950 Å, b = 8.428 Å, and c = 6.005 Å.

APPENDIX C

X-ray Powder Diffraction Data of the $PbZrO_3$-$BiFeO_3$ System

Notes:

1. All x-ray patterns are based on copper $K\alpha$ radiation with a wavelength of 1.542 Å.

2. The indices of the x-ray patterns of each composition include only the main phase (see Table VI); the structure is indicated in each table.

3. In each composition of the system, from 100 to 30 mole percent $PbZrO_3$, a is primarily calculated from the d value of the (400) line, b = 2a and c is determined from the (004) line: from 25 to 0 mole percent $PbZrO_3$, a is calculated primarily from the (300) line.

4. The rhombohedral angle α is calculated from the equation[14]

$$\text{Cos}\ \alpha = \frac{d_{hkl} - d_{hkl}}{2d_{hkl}} \quad \frac{h^2 + k^2 + l^2}{(h + k)\, l}$$

   The pair of lines, d_{hkl} and d_{hkl}, used for each composition in the rhombohedral phase is indicated in the respective tables.

5. The samples used here for each composition are the same as in Table VI.

A. COMPOSITION: 100% $PbZrO_3$

Structure: Orthorhombic I.
Parameters: a = 5.873 Å, b = 11.746 Å, c = 8.228 Å.

2 θ	d (Å)	I/I_o	hkl
16.86	5.254	4	110
21.37	4.154	10.4	120
21.57	4.116	6	002
27.36	3.262	5	130
27.45	3.257	5	112
29.10	3.067	4	131
30.50	2.928	100	200, 040
31.37	2.849	5	210
32.57	2.747	2	041, 201
35.05	2.558	2	132
37.60	2.390	14	042, 202
38.41	2.341	4	050, 230
43.52	2.078	26	240
43.98	2.057	15	004
46.98	1.932	3	310
48.97	1.858	3	320
49.40	1.843	3	124
52.22	1.750	6	330
54.08	1.694	34	322
54.42	1.685	23	204, 044
55.00	1.668	3	214
57.10	1.612	4	332
59.60	1.550	1	-
61.56	1.505	2	350
63.28	1.468	7	400
63.56	1.463	13	135
63.74	1.459	9	244
66.15	1.4114	2	352
68.14	1.3749	3	412
70.60	1.3329	1	026
71.79	1.3137	9	440
72.52	1.3025	8	432
76.57	1.2432	1	450
78.60	1.2171	1	-
80.09	1.1972	5	335
80.32	1.1943	4	236
84.70	1.1434	2	434
86.34	1.1258	3	530

A. (Cont'd)

2θ	d (Å)	I/I_o	hkl
87.70	1.1118	5	531
88.00	1.1088	8	522
88.47	1.1041	7	444
88.78	1.1011	4	326

B. COMPOSITION: 95% $PbZrO_3$-5% $BiFeO_3$

Structure: Orthorhombic I.
Parameters: a = 5.869 Å, b = 11.738 Å, c = 8.223 Å.

2θ	d (Å)	I/I_o	hkl
16.88	5.248	2	110
21.38	4.152	12	120
21.59	4.113	7	002
27.53	3.237	4	112
28.20	3.162	2	(ZrO_2)
30.52	2.927	100	200, 040
31.42	2.845	4	210
32.60	2.744	1	201, 041
35.14	2.552	1	132
37.62	2.389	13	202, 042
38.46	2.339	2	230, 050
43.58	2.075	22	240
44.01	2.056	12	004
47.02	1.931	2	310
49.09	1.854	2	320
49.46	1.841	2	124
52.27	1.749	4	330
54.14	1.693	25	322
54.41	1.685	18	204, 044
55.00	1.668	2	214
57.27	1.607	2	332
61.65	1.503	1	350
63.33	1.4673	5	400
63.62	1.4613	9	135
63.78	1.4580	8	244
68.29	1.3723	2	412
71.89	1.3121	6	440

B. (Cont'd)

2 θ	d (Å)	I/I$_o$	hkl
72.58	1.3014	4	432
76.64	1.2422	1	450
80.31	1.1944	2	335
80.55	1.1915	2	236
84.70	1.1434	1	434
86.60	1.1231	1	530
88.05	1.1083	4	531
88.21	1.1067	5	522
88.61	1.1028	5	444
88.93	1.0996	3	326

C. COMPOSITION: 90.47% $PbZrO_3$-9.53% $BiFeO_3$

Structure: Orthorhombic I
Parameters: a = 5.864 Å, b = 11.728 Å, c = 8.216 Å.

2 θ	d (Å)	I/I$_o$	hkl
16.90	5.241	3	110
21.42	4.145	13	120
21.60	4.111	9	002
27.56	3.234	4	112
28.19	3.163	2	(ZrO_2)
30.54	2.925	100	200, 040
31.46	2.839	4	210, (ZrO_2)
35.20	2.554	2	132
37.65	2.387	14	202, 042
38.49	2.337	3	230, 050
43.62	2.073	21	240
44.06	2.054	11	004
47.16	1.928	4	310
49.15	1.852	7	320
49.50	1.840	6	124
52.32	1.747	8	330
54.18	1.691	60	322
54.39	1.685	54	204, 044
55.06	1.666	7	214
57.18	1.610	6	332

C. (Cont'd)

2θ	d (Å)	I/I_o	hkl
61.90	1.4977	2	350
63.39	1.4660	10	400
63.67	1.4602	22	135
68.40	1.3703	4	412
72.04	1.3098	14	440
72.68	1.2998	10	432
76.73	1.2410	2	450
80.45	1.1927	7	335
80.60	1.1909	7	236
86.72	1.1219	4	530
88.10	1.1078	9	531
88.32	1.1056	13	522
88.68	1.1021	13	444
89.01	1.0988	6	326

D. COMPOSITION: 85% $PbZrO_3$-15% $BiFeO_3$

Structure: Orthorhombic I.
Parameters: a = 5.850 Å, b = 11.700 Å, c = 8.212 Å.

2θ	d (Å)	I/I_o	hkl
17.00	5.211	3	110
21.48	4.133	15	120
21.62	4.107	9	002
27.59	3.230	5	112
28.19	3.163	4	(ZrO_2)
30.59	2.920	100	200, 040
31.46	2.841	5	(ZrO_2)
37.72	2.383	13	202, 042
43.73	2.068	22	240
44.08	2.053	10	004
49.18	1.851	4	320
52.55	1.740	3	330
54.34	1.687	26	322
54.50	1.682	19	204, 044
63.56	1.4625	15	400
63.77	1.4582	27	135
63.98	1.4537	16	135
68.50	1.3686	6	412

2 θ	d (Å)	I/I_o	hkl
72.19	1.3074	16	440
72.78	1.2983	11	432
80.64	1.1904	10	335
88.48	1.1040	12	522
88.82	1.1017	12	444

E. COMPOSITION: 81.81% $PbZrO_3$-18.19% $BiFeO_3$

Structure: Orthorhombic I.
Parameters: a = 5.842 Å, b = 11.684 Å, c = 8.214 Å

2 θ	d (Å)	I/I_o	hkl
17.08	5.248	2	110
21.48	4.133	14	120
21.61	4.109	13	002
27.60	3.229	3	112
18.19	3.163	4	(ZrO_2)
30.60	2.919	100	040, 200
31.46	2.841	5	(ZrO_2)
37.77	2.380	14	202, 042
43.79	2.066	20	240
44.04	2.054	10	004
49.30	1.847	3	320
52.60	1.738	1	330
54.46	1.683	23	332
54.55	1.681	20	204, 044
63.66	1.4605	5	400
63.85	1.4566	9	135
64.02	1.4531	6	244
72.28	1.3060	5	440
62.91	1.2962	4	432
80.68	1.1989	3	335
88.72	1.1017	5	522

F. COMPOSITION: 80% $PbZrO_3$-20% $BiFeO_3$

Structure: Orthorhombic II.
Parameters: a = 5.830 Å, b = 11.660 Å, c = 8.246 Å.

2 θ	d (Å)	I/I_o	hkl
21.53	4.124	2	002, 120
27.60	3.229	2	130
28.18	3.173	3	(ZrO_2)
30.62	2.917	100	200, 040
37.70	2.384	11	042, 202
43.88	2.062	22	004, 240
49.31	1.847	3	124
54.52	1.682	24	322, 044, 204
63.80	1.4576	8	400
72.50	1.3026	5	422
80.80	1.1884	3	404
88.82	1.1007	2	444

G. COMPOSITION: 75% $PbZrO_3$-25% $BiFeO_3$

Structure: Orthorhombic II.
Parameters: a = 5.820 Å, b = 11.640 Å, c = 8.230 Å.

2 θ	d (Å)	I/I_o	hkl
21.59	4.113	20	002, 120
27.64	3.225	4	130
28.18	3.1639	4	(ZrO_2)
30.68	2.912	100	200, 040
31.52	2.8359	1	(ZrO_2)
37.77	2.380	12	042, 202
43.97	2.058	22	004, 240
47.63	1.908	2	-
49.33	1.846	3	124
54.52	1.682	25	322, 044, 204
63.93	1.4549	9	400
72.55	1.3018	6	422
80.90	1.1872	3	404
89.02	1.0987	5	444

H. COMPOSITION: 70% $PbZrO_3$-30% $BiFeO_3$

Structure: Orthorhombic II.
Parameters: a = 5.808 Å, b = 11.616 Å, c = 8.214 Å.

2 θ	d (Å)	I/I_o	hkl
21.62	4.107	18	002, 120
27.80	3.206	4	130
28.18	3.164	4	(ZrO_2)
30.72	2.908	100	200, 040
31.52	2.836	3	(ZrO_2)
31.79	2.812	2	210
37.83	2.376	13	040, 202
44.06	2.054	24	004, 240
49.55	1.838	3	124
54.68	1.677	26	322, 044, 204
64.07	1.4521	8	400
62.68	1.2998	6	422
80.00	1.1983	2	404
89.11	1.0979	4	444

I. COMPOSITION: 60% $PbZrO_3$-40% $BiFeO_3$

Structure: Orthorhombic II.
Parameters: a = 5.781 Å, b = 11.562 Å, c = 8.175 Å.

2 θ	d (Å)	I/I_o	hkl
21.73	4.086	19	002, 120
27.82	3.206	6	130
28.20	3.162	7	(ZrO_2)
30.91	2.891	100	200, 040
31.54	2.834	7	(ZrO_2)
31.82	2.810	2	210
38.08	2.361	13	042, 202
44.28	2.044	23	004, 240
49.90	1.826	4	124
54.98	1.669	24	322, 044, 204
64.41	1.4453	8	400
71.14	1.3241	5	422
81.62	1.1786	7	404
89.60	1.0931	10	444

J. COMPOSITION 50% $PbZrO_3$-50% $BiFeO_3$

Structure: Orthorhombic II.
Parameters: a = 5.751 Å, b = 11.502 Å, c = 8.133 Å.

2 θ	d (Å)	I/I_o	hkl
21.83	4.068	23	002, 120
27.84	3.202	7	130
28.19	3.165	9	(ZrO_2)
31.07	2.876	100	200, 040
31.75	2.816	9	-
32.38	2.763	2	210
34.19	2.620	1	-
38.21	2.353	14	-
44.52	2.033	23	004, 240
45.58	1.989	1	-
47.77	1.923	1	-
50.04	1.821	4	124
53.98	1.697	2	-
55.24	1.661	23	322, 044, 204
64.79	1.4377	7	400
73.56	1.2864	5	422
81.91	1.1751	2	404
90.22	1.0872	4	444

K. COMPOSITION: 35% $PbZrO_3$-65% $BiFeO_3$

Structure: Orthorhombic II.
Parameters: a = 5.679 Å, b = 11.358 Å, c = 8.029 Å.

2 θ	d (Å)	I/I_o	hkl
22.14	4.012	26	002, 120
27.94	3.191	8	130
28.20	3.162	17	(ZrO_2)
31.48	2.839	100	200, 040
32.57	2.747	2	210
38.76	2.321	14	-
45.12	2.008	19	004, 240
48.24	1.885	1	-
50.06	1.821	3	-
50.80	1.796	5	124
53.78	1.703	2	-
56.04	1.640	21	322, 044, 204
65.72	1.4197	4	400
74.78	1.2681	4	422

L. COMPOSITION: 30% $PbZrO_3$-70% $BiFeO_3$

Structure: Orthorhombic II.
Parameters: a = 5.655 Å, b = 11.310 Å, c = 7.990 Å.

2 θ	d (Å)	I/I_o	hkl
22.25	3.993	30	002, 120
28.07	3.176	7	130
28.37	3.143	14	-
31.62	2.827	100	200, 040
32.59	2.745	3	210
38.99	2.308	21	042, 202
45.32	1.999	18	004, 240
46.00	1.971	2	-
48.24	1.885	2	-
50.05	1.820	2	-
51.02	1.822	5	124
53.70	1.7054	3	-
54.68	1.6771	2	-
56.28	1.633	21	322, 040, 204
66.03	1.4137	7	400
75.13	1.4133	4	422
83.55	1.1562	1	404
92.21	1.0689	2	444

M. COMPOSITION: 25% $PbZrO_3$-75% $BiFeO_3$

Structure: Rhombohedral
Parameters: a = 3.985 Å, α* = ?

2 θ	d (Å)	I/I_o	hkl
22.29	3.985	27	100
27.88	3.197	9	(γ-Bi_2O_3)
28.20	3.162	10	(ZrO_2)
28.78	3.099	3	-
31.69	2.821	100	110, $10\bar{3}$
33.01	2.975	2	(γ-Bi_2O_3)
38.27	2.411	2	111
39.12	2.301	19	101

* See Table VI.

M. (Cont'd)

2 θ	d (Å)	I/I_o	hkl
45.46	1.994	19	200
46.28	1.960	4	140
48.60	1.872	2	-
51.15	1.784	6	201
54.79	1.674	2	-
56.48	1.628	21	$11\bar{2}, 21\bar{1}$
66.26	1.4093	3	$20\bar{2}$
70.88	1.3284	1	300
75.25	1.2617	3	$30\bar{1}$
84.23**	1.1486	1	-
92.64	1.0650	2	312

** This peak is broad and its 2 θ value can not be determined accurately.

N. COMPOSITION: 20% $PbZrO_3$-80% $BiFeO_3$

Structure: Rhombohedral.
Parameters: a = 3.981 Å, α = 89.290° (calculated from the lines of $211, 21\bar{1}$).

2 θ	d (Å)	I/I_o	hkl
22.32	3.980	31	100
27.89	3.196	11	(γ-Bi_2O_3)
28.19	3.163	8	(ZrO_2)
28.77	3.100	3	-
31.75	2.816	100	$110, 10\bar{3}$
32.80	2.733	5	-
37.37	2.404	1	-
38.80	2.319	3	111
39.15	2.299	17	101
45.55	1.990	20	200
46.25	1.961	6	140
50.66	1.800	4	-
51.29	1.780	6	201
54.78	1.674	4	-
55.99	1.641	6	211
56.54	1.626	16	$11\bar{2}, 21\bar{1}$

N. (Cont'd)

2θ	d (Å)	I/I_o	hkl
61.93	1.4970	3	-
66.45	1.4058	6	$20\bar{2}$
70.98	1.3267	3	300
75.35	1.2899	4	$30\bar{1}$

O. COMPOSITION: 15% $PbZrO_3$-85% $BiFeO_3$

Structure: Rhombohedral
Parameters: a = 3.976 Å, α = 89.283° (calculated from the lines of 211, $21\bar{1}$).

2θ	d (Å)	I/I_o	hkl
21.30	4.168	3	-
22.34	3.976	41	100
24.11	3.688	3	-
27.88	3.197	17	(γ-Bi_2O_3)
28.19	3.163	6	(ZrO_2)
29.09	3.065	4	-
30.98	2.884	7	-
31.79	2.812	100	110, $10\bar{3}$
38.82	2.318	7	111
39.22	2.295	17	101
45.61	1.987	17	200
46.28	1.960	10	104
51.05	1.785	9	210
51.35	1.778	11	201
54.93	1.670	5	-
56.18	1.636	10	211
56.77	1.621	20	$21\bar{1}$, $11\bar{2}$
57.48	1.602	8	-
66.68	1.4127	6	$20\bar{2}$
70.56	1.3254	4	300
75.56	1.2573	5	$30\bar{1}$
79.78	1.2010	3	$31\bar{1}$

P. COMPOSITION: 11.11% $PbZrO_3$-88.89% $BiFeO_3$

Structure: Rhombohedral
Parameters: a = 3.974 Å, α = 89.276° (calculated from the lines of 211, $21\bar{1}$).

2 θ	d (Å)	I/I$_o$	hkl
22.34	3.973	45	100
24.81	3.586	2	-
27.90	3.195	9	(γ-Bi_2O_3)
28.19	3.162	4	(ZrO_2)
29.90	2.986	2	-
31.71	2.819	64	110
31.90	2.803	100	$10\bar{3}$
33.04	2.708	2	(γ-Bi_2O_3)
35.30	2.540	4	-
38.87	2.315	6	111
39.33	2.289	22	101
45.64	1.986	20	200
46.33	1.958	7	104
51.16	1.784	13	210
51.45	1.775	11	201
55.07	1.666	5	-
56.22	1.635	10	211
56.80	1.620	25	$21\bar{1}$, $11\bar{2}$
61.88	1.4981	2	-
66.83	1.3987	7	$20\bar{2}$
70.56	1.3336	5	221
71.10	1.3248	6	300
75.59	1.2568	6	310
75.78	1.2542	5	$30\bar{1}$
79.35	1.2064	3	$31\bar{1}$
80.07	1.1974	3	311

Q. COMPOSITION: 5% $PbZrO_3$-95% $BiFeO_3$

Structure: Rhombohedral
Parameters: a = 3.965 Å, α = 89.266° (calculated from the lines of 321, $32\bar{1}$).

2 θ	d (Å)	I/I$_o$	hkl
22.49	3.950	53	110
24.82	3.584	3	-
27.88	3.197	11	(γ-Bi_2O_3)

Q. (Cont'd)

2 θ	d (Å)	I/I_o	hkl
28.22	3.160	6	$Bi_2O_3 \cdot 2Fe_2O_3$
28.98	3.079	4	$Bi_2O_3 \cdot 2Fe_2O_3$
29.77	2.999	2	$Bi_2O_3 \cdot 2Fe_2O_3$
31.82	2.810	96	110
32.09	2.787	100	$10\bar{3}$
33.04	2.709	6	(γ-Bi_2O_3)
39.00	2.308	16	111
39.48	2.281	29	101
45.78	1.980	39	200
47.03	1.931	3	104
51.32	1.779	32	210
51.74	1.765	17	201
52.42	1.744	2	-
56.37	1.631	27	211
56.80	1.620	23	$21\bar{1}$
56.99	1.615	46	112
57.02	1.614	1	-
61.84	1.521	2	-
66.24	1.4097	7	220
66.97	1.3961	12	$20\bar{2}$
70.60	1.3329	10	221
71.30	1.3216	10	300
73.75	1.2835	1	-
75.65	1.2560	12	310
75.89	1.2560	12	$30\bar{1}$
79.65	1.2027	5	311
80.24	1.1953	7	$31\bar{1}$
83.55	1.1562	1	-
84.80	1.1432	4	222
88.36	1.1052	6	320
89.37	1.0953	3	302
92.31	1.0680	7	321
93.15	1.0606	10	$32\bar{1}$
93.60	1.0566	12	312

R. COMPOSITION: 100% $BiFeO_3$

Structure: Rhombohedral
Parameters: a = 3.951 Å, α = 89.265° (calculated from the lines of 321, 32$\bar{1}$).

2 θ	d (Å)	I/I_o	hkl
14.74	6.005	6	($Bi_2O_3 \cdot 2Fe_2O_3$)
22.52	3.945	76	100
24.91	3.571	9	(γ-Bi_2O_3)
27.92	3.193	26	(γ-Bi_2O_3)
28.24	3.157	26	($Bi_2O_3 \cdot 2Fe_2O_3$)
28.98	3.078	17	($Bi_2O_3 \cdot 2Fe_2O_3$)
30.54	2.925	4	(γ-Bi_2O_3)
31.00	2.882	6	($Bi_2O_3 \cdot 2Fe_2O_3$)
31.92	2.801	100	110
32.16	2.779	86	10$\bar{3}$
33.06	2.707	25	(γ-Bi_2O_3)
33.76	2.653	16	($Bi_2O_3 \cdot 2Fe_2O_3$)
37.00	2.428	5	($Bi_2O_3 \cdot 2Fe_2O_3$)
37.70	2.384	7	($Bi_2O_3 \cdot 2Fe_2O_3$), (γ-Bi_2O_3)
39.11	2.301	17	111
39.60	2.274	36	101
42.02	2.148	5	(γ-Bi_2O_3)
43.85	2.063	4	(γ-Bi_2O_3)
45.96	1.973	46	200
47.23	1.923	14	104, ($Bi_2O_3 \cdot 2Bi_2O_3$)
49.70	1.833	7	($Bi_2O_3 \cdot 2Fe_2O_3$)
51.52	1.773	39	210
51.78	1.764	36	201
52.59	1.739	12	(γ-Bi_2O_3)
54.33	1.687	6	(γ-Bi_2O_3)
55.99	1.641	9	(γ-Bi_2O_3)
56.55	1.626	29	211, ($Bi_2O_3 \cdot 2Bi_2O_3$)
57.00	1.614	38	21$\bar{1}$
57.18	1.610	50	11$\bar{2}$
62.26	1.4899	6	(γ-Bi_2O_3)
66.48	1.4052	10	220
67.17	1.3924	16	20$\bar{2}$
70.67	1.3318	10	221
71.58	1.3171	16	300
71.91	1.3119	12	21$\bar{2}$
73.80	1.2829	5	-
75.73	1.2548	17	310

R. (Cont'd)

2θ	d (Å)	I/I_o	hkl
76.22	1.2480	23	$30\bar{1}$
79.92	1.9993	9	311
80.54	1.1916	12	$31\bar{1}$
85.20	1.1379	10	222
86.93	1.1197	7	-
88.78	1.1011	19	320
89.53	1.0938	12	302
92.58	1.0656	8	321
93.42	1.0582	14	$32\bar{1}$
93.95	1.0536	25	312

VITA

Pen-chu Chou was born in Chianghsi, China, on January 1, 1936. He received his elementary and secondary education in China, and graduated from Tunghai University at Taiwan, China in July 1961, with a Bachelor of Science in Chemistry.

In February of 1964, he enrolled in Chemistry at the Graduate School of the University of Missouri at Rolla. From September 1964 to December 1965, he was appointed a research assistant in the Chemistry Department with funds provided by the U. S. Atomic Energy Commission.